Accepted Manuscript

High fat diet-induced modifications in membrane lipid and mitochondrial-membrane protein signatures precede the development of hepatic insulin resistance in mice

M. Kahle , A. Schäfer , A. Seelig , J. Schultheiß , M. Wu , M. Aichler , J. Leonhardt , B. Rathkolb , J. Rozman , H. Sarioglu , S.M. Hauck , M. Ueffing , E. Wolf , G. Kastenmueller , J. Adamski , A. Walch , M Hrabé de Angelis , S. Neschen

PII: S2212-8778(14)00186-0

DOI: 10.1016/j.molmet.2014.11.004

Reference: MOLMET 188

To appear in: *Molecular Metabolism*

Received Date: 21 October 2014

Revised Date: 5 November 2014

Accepted Date: 7 November 2014

Please cite this article as: Kahle M, Schäfer A, Seelig A, Schultheiß J, Wu M, Aichler M, Leonhardt J, Rathkolb B, Rozman J, Sarioglu H, Hauck S, Ueffing M, Wolf E, Kastenmueller G, Adamski J, Walch A, de Angelis MH, Neschen S, High fat diet-induced modifications in membrane lipid and mitochondrial-membrane protein signatures precede the development of hepatic insulin resistance in mice, *Molecular Metabolism* (2014), doi: 10.1016/j.molmet.2014.11.004.

High fat diet-induced modifications in membrane lipid and mitochondrial-membrane protein signatures precede the development of hepatic insulin resistance in mice

M Kahle[1,7], A Schäfer[2,7], A Seelig[1], J Schultheiß[1,7], M Wu[1,7], M Aichler[6], J Leonhardt[5], B Rathkolb[3,4], J Rozman[3,7], H Sarioglu[2], SM Hauck[2,7], M Ueffing[2,7], E Wolf[4], G Kastenmueller[5], J Adamski[1,8], A Walch[6], M Hrabé de Angelis[1,3,7], S Neschen[1,3,7]

[1] Institute of Experimental Genetics, Helmholtz Zentrum München, German Research Center for Environmental Health, Ingolstädter Landstrasse 1, 85764 Neuherberg/Munich, Germany.

[2] Research Unit Protein Science, Helmholtz Zentrum München, German Research Center for Environmental Health, Ingolstädter Landstraße 1, 85764 Neuherberg/Munich, Germany.

[3] German Mouse Clinic, Institute of Experimental Genetics, Helmholtz Zentrum München, German Research Center for Environmental Health, Ingolstädter Landstraße 1, 85764 Neuherberg/Munich, Germany

[4] Chair for Molecular Animal Breeding and Biotechnology, Gene Center, Ludwig-Maximilians-Universität München, Feodor Lynen-Straße 25, 81377 Munich, Germany

[5] Institute of Bioinformatics and Systems Biology, Helmholtz Zentrum München, German Research Center for Environmental Health, Ingolstädter Landstraße 1, 85764 Neuherberg/Munich, Germany.

[6] Research Unit Analytical Pathology, Helmholtz Zentrum München, German Research Center for Environmental Health, Ingolstädter Landstraße 1, 85764 Neuherberg/Munich, Germany.

[7] Member of German Center for Diabetes Research (DZD), Ingolstädter Landstraße 1, 85764 Neuherberg/Munich, Germany

[8] Institute of Experimental Genetics, Genome Analysis Center, Helmholtz Zentrum München, German Research Center for Environmental Health, Ingolstädter Landstraße 1, 85764 Neuherberg/Munich, Germany.

CORRESPONDING AUTHOR: Michaela Aichler, Research Unit Analytical Pathology, Helmholtz Zentrum München, German Research Center for Environmental Health, Ingolstädter Landstraße 1, 85764 Neuherberg/Munich, Germany; Tel: 0049.89.2637; Fax: 0049.89.3187. 3349; Email: michaela.aichler@helmholtz-muenchen.de

ABBREVIATIONS: 2-[^{14}C]DG, 2-[1-^{14}C]deoxyglucose; GIR, glucose infusion rate; Rd, rate of disappearance; Ra, rate of appearance; EGP, endogenous (hepatic) glucose production; AUC, area under the curve; HF, high-fat diet; LF, low-fat diet; WAT, white adipose tissue; ROS, reactive oxygen species; DAG, diacylglycerol; TAG, triacylglycerol; WAT, white adipose tissue; NEFA, non-esterified fatty acids; ALT, alanine aminotransferase; Basal, 17 hr fasting; Rg, glucose metabolic index; PCaa, diacylglycerophosphocholine; PCae, glycerophosphocholine; lysoPC, lysophosphatidylcholines; SM, sphingolipid; B, basal; IS, insulin-stimulated

ABSTRACT

Objective: Excess lipid intake has been implicated in the pathophysiology of hepatosteatosis and hepatic insulin resistance. Lipids constitute approximately 50% of the cell membrane mass, define membrane properties, and create microenvironments for membrane-proteins. In this study we aimed to resolve temporal alterations in membrane metabolite and protein signatures during high-fat diet (HF)-mediated development of hepatic insulin resistance.

Methods: We induced hepatosteatosis by feeding C3HeB/FeJ male mice a HF enriched with long-chain polyunsaturated C18:2n6 fatty acids for 7, 14, or 21 days. Longitudinal changes in hepatic insulin sensitivity were assessed *via* the euglycemic-hyperinsulinemic clamp, in membrane lipids *via* t-metabolomics- and membrane proteins *via* quantitative proteomics-analyses, and in hepatocyte morphology *via* electron microscopy. Data were compared to those of age- and litter-matched controls maintained on a low-fat diet.

Results: Excess long-chain polyunsaturated C18:2n6 intake for 7 days did not compromise hepatic insulin sensitivity, however induced hepatosteatosis and modified major membrane lipid constituent signatures in liver, e.g. increased total unsaturated, long-chain fatty acid-containing acyl-carnitine or membrane-associated diacylglycerol moieties and decreased total short-chain acyl-carnitines, glycerophosphocholines, lysophosphatidylcholines, or sphingolipids. Hepatic insulin sensitivity tended to decrease within 14 days HF-exposure. Overt hepatic insulin resistance developed until day 21 of HF-intervention and was accompanied by morphological mitochondrial abnormalities and indications for oxidative stress in liver. HF-feeding progressively decreased the abundance of protein-components of all mitochondrial respiratory chain complexes, inner and outer mitochondrial membrane substrate transporters independent from the hepatocellular mitochondrial volume in liver.

Conclusions: We assume HF-induced modifications in membrane lipid- and protein-signatures prior to and during changes in hepatic insulin action in liver alter membrane

properties – in particular those of mitochondria which are highly abundant in hepatocytes. In turn, a progressive decrease in the abundance of mitochondrial membrane proteins throughout HF-exposure likely impacts on mitochondrial energy metabolism, substrate exchange across mitochondrial membranes, contributes to oxidative stress, mitochondrial damage, and the development of insulin resistance in liver.

INTRODUCTION

Type 2 diabetes is a growing global phenomenon and considered a major complication in most overweight patients with non-alcoholic fatty liver disease (NAFLD); *vice versa*, type 2 diabetes is frequently complicated by NAFLD [1]. Excessive short-term or chronic fat intake expands hepatic lipid stores and impairs hepatic insulin action. In turn, insulin resistance in liver is thought to act as a driving force in both, the pathogenesis of type 2 diabetes and NAFLD [2-4].

Various bioactive lipid classes – such as fatty acids, acyl-carnitines, diacylglycerols, phospholipids, or ceramides – have been implicated in the pathophysiology of hepatic insulin resistance in animal models and humans [2,5-9]. Fatty acids are central regulators of hepatic lipid metabolism as they modulate the activity of several transcription factors, e.g. peroxisome proliferator-activated receptors, hepatic nuclear factors, sterol regulatory element binding protein-1c, retinoid X receptor, or liver X receptor [10]. Diacylglycerols, their break-down products and ceramides act as first and second messengers and interfere with insulin signaling in liver [2,6,11,12]. In addition, lipids constitute approximately half of the mass of most animal cell membranes, the latter dividing the extra- and intracellular environment thereby restricting biological reactions, their educts and products [13]. Phospholipids, such as phosphatidylcholines and phosphatidylethanolamines, are the most abundant eukaryotic membrane lipids. They consist of a polar head group and two hydrophobic hydrocarbon tails, the latter usually fatty acids. Due to their amphipathic nature and geometry, polar lipids spontaneously align side-by-side thereby aggregating into semipermeable membranes. Diacylglycerols transiently accumulate in membranes and facilitate membrane fusion.

The lipid composition of the diet modulates lipid signatures of membranes and contributes to the creation of microenvironments in membranes that account for protein enrichment or dispersion. Membrane properties are substantially modulated by both, the chain lengths and the number of double bonds of the incorporated fatty acids [15]. For example,

phosphatidylcholine containing a C18:0 acyl-chain in the sn-1 and sn-2 position has a melting point of approximately 55 °C. At mammalian body temperatures it therefore exists in a solid aggregation state. If the C18:0 acyl-chain in the sn-2 position is replaced by 18:2n-6, it maintains a liquid crystalline state until approximately 15 °C [16]. Sphingolipids aggregate in microdomains or rafts that float within the membrane. As the saturated hydrocarbon tails of sphingolipids are usually longer and straighter than those of other membrane lipids, they accommodate the largest membrane proteins [13].

Recent advances have been made to more closely investigate the role of various bioactive lipid classes in the pathogenesis of type 2 diabetes and hepatosteatosis. Given the structural and functional importance of membranes, modifications in membrane lipid and protein signatures might play a role in the development of high fat diet (HF)-induced hepatic insulin resistance. However, whether early qualitative and quantitative changes in membrane-associated lipid species and proteins precede, accompany or result in HF-induced hepatic insulin resistance is not clear.

Therefore, we assessed comprehensive, longitudinal alterations in major membrane lipid components with targeted-metabolomics and membrane-associated proteins using discovery proteomics in livers of mice during developing HF-mediated hepatic insulin resistance.

MATERIAL AND METHODS

Mice and study design. C3HeB/FeJ (C3H) mice were housed under standard *vivarium* conditions (12:12 light-dark-cycle) and maintained on low-fat diet (LF, 13% fat-derived calories, 17 kJ/g, Diet#1310, Altromin, Germany). At an age of 14 weeks, male mice were matched for body mass and litter, and single-housed in cages including a domehouse and nestlet. For 7, 14, or 21 days, mice had free access to a previously published high-fat diet (HF, 58% fat-derived calories, 25 kJ/g, Ssniff, Germany) containing ~78% C18:2n-6 fatty acid [17]. The HF was exchanged every third day. One group of mice (REC) was treated with HF for 14 days and switched back to LF for 7 days. Initial body mass-, age-, and litter-matched control groups were continued on LF for 7, 14, or 21 days. Body mass and composition (MiniSpec LF50, Bruker Optics, Germany) were measured one day prior to the experiment start and end. If not stated otherwise, at the study end mice were killed with isoflurane between 9-11AM in the random-fed state. *V. cava* blood was obtained, immediately centrifuged at 4 °C, and plasma aliquots were frozen in liquid nitrogen. Liver, *M. gastrocnemius*, epididymal and mesenteric white adipose tissue pads were dissected. Some organs were weighed, and immediately freeze-clamped in liquid nitrogen. Livers were ground in liquid nitrogen, and homogenates stored at -80 °C for further analyzes. All animals received humane care according to criteria outlined in the National Academy of Sciences Guide for the Care and Use of Laboratory Animals. All animal experiments were approved by the Upper-Bavarian district government (Regierung von Oberbayern Gz.55.2-1-54-2532-4-11).

Plasma and liver biochemical analyses. Plasma immunoreactive insulin was determined with a Mouse Insulin ELISA (Mercodia, Sweden) and all other plasma parameters with an AU400 autoanalyzer (Olympus, Germany) using adapted reagents from Beckman Coulter, Wako

Chemicals, or Randox Laboratories. Plasma triacylglycerol (Sigma Diagnostics, USA), and non-esterified fatty acids (NEFA-C, Wako Pure Chemicals, Japan) were measured with reagent kits. For liver triacylglycerol quantification approximately 50 mg ground liver aliquots were homogenized (TissueLyserII Qiagen, Germany) with 1 ml 5% Triton-X100. Triacylglycerol concentrations were quantified enzymatically with a commercial kit according to the manufacturer's instructions (Biovision, USA).

Euglycemic-hyperinsulinemic clamps. A cohort of mice was equipped with permanent jugular vein-catheters (i.p. ketamine/xylazine 80/10 mg/kg). After six to seven days recovery ~17-hour fasting, conscious mice were subjected to euglycemic-hyperinsulinemic clamps. Blood samples were obtained after single initial tail biopsy by gently massaging tails and taping tips between sampling. For determination of fasting (basal) whole-body glucose turnover rates ($EndoR_a$) a primed-continuous [3-^{3}H]glucose infusion (1.85 kBq/min) was applied for 120 min and a blood sample for basal plasma glucose, [3-^{3}H]glucose, and insulin measurements was withdrawn in the final 10 min. Clamps were started with a continuous [3-^{3}H]glucose (3.7 kBq/min) and insulin infusion (24 pmol/kg*min^{-1}; HumulinR, Lilly, USA). Blood glucose was measured every 10 min (Bayer Contour, Germany) and blood glucose fluctuations were adjusted by varying the rate of a 20%-glucose solution (GIR). Between min 90 and 120, four blood samples were collected to estimate insulin-mediated suppression of endogenous glucose appearance ($EndoR_a$), whole-body glucose disappearance rates (R_d) and plasma insulin concentrations. Between minute 0 of the end of the clamp blood loss was compensated by infusing donor blood cells at a rate of 3 µl/min. Blood was obtained from male, LF-fed littermates. To prepare the infusion solution, the donor blood was gently centrifuged, the supernatant discarded, blood cells were re-suspended in sterile 0.9% NaCl-solution and all steps were repeated once more. All infusions were performed with CMA402-pumps (Axel Semrau, Germany) and radioisotopes were purchased from Perkin Elmer

(Boston, USA). At the end of experiments animals were killed with i.v. ketamine/xylazine. Liver, *M. gastrocnemius*, heart, and epididymal white adipose tissue were immediately dissected, freeze-clamped, and stored at -80 °C. Plasma analyses and glucose flux calculations were performed as previously described [18]. Phospho-AKT (Ser473) and total AKT protein were assessed in liver homogenates with a multiarray-assay and a SECTOR Imager6000 according to the manufacturer's protocol (K15100D-1, MesoScaleDiscovery, USA).

Targeted-metabolomics. Measurements in plasma and liver homogenates were conducted with the Absolute*IDQ*™ p180 kit (Biocrates Life Sciences, Austria) according to the manufacturer's manual UM-P180 and as previously described [19]. Sample handling was performed by a Microlab STAR™ robot (Hamilton, Switzerland) and Ultravap nitrogen evaporator (Porvair Sciences, UK). Mass spectrometric (MS) analyses were performed with API4000 LC/MS/MS System (AB Sciex, Germany) equipped with 1200 Series HPLC (Agilent, Germany) and HTC-PAL autosampler (CTC Analytics, Switzerland) software-controlled by Analyst1.5.1. Internal standards served as reference for calculation of metabolite concentrations. Data evaluation for metabolite concentration quantification and quality assessment was performed with Met*IDQ*™ software. Several biomarkers in this manuscript are referred to in the Biocrates MetaDis*IDQ*™ Kit product information 2010-10-06 and application note BB-MD-1. Due to the instability of effector molecules and their products oxidative stress is difficult to measure. Among amino acids, methionine ranks among the most sensitive to oxidation. According to a clinical study sulfoxidation of methionine markedly correlated with chronic kidney disease stages and the methionine sulfoxide/methionine (Met-SO/Met) ratio was suggested to represent a stable endpoint of oxidative stress [20].

Liver diacylglycerol measurement. At the study end, a separate cohort of six-hour fasting mice was killed with isoflurane between 9-11 a.m. Diacylglycerol was extracted from liver homogenates by homogenization in a buffer containing 20 mM Tris-HCl, 1mM EDTA, 0.25 mM EGTA, 250 mM sucrose, 2 mM phenylmethylsulfonyl fluoride, and a protease inhibitor mixture (Roche). Diacylglycerol species were measured by LC/MS/MS [21].

Proteomics. Proteins from frozen liver homogenates were extracted by mechanical homogenization (Precellys24, Bertin Technologies). Membrane vesicles were harvested at 100.000g 4 °C for 30 min and a carbonate extraction of membrane proteins was performed as described earlier [22] [23]. Protein pellets were resuspended in 50 mM Tris pH 8.5 0.2 % Rapigest (Waters) and subjected to tryptic digestion. Cysteines were reduced using DTT and alkylated using iodoacetamide. Proteins were digested with 5 µg trypsin for 18 hours at 37 °C. Peptides were separated by reversed-phase chromatography (PepMap, 0.075x150 mm, 3 µm 100 A° pore size, LC Packings) with a 170-min gradient using 2 % acetonitrile in 0.1 % formic acid in water (A) and 0.1 % formic acid in 98 % acetonitrile (B) at 250 nl/min flow rate. The gradient settings were subsequently: 0–140 min: 5-31 % B. 140-145 min: 31-99 % B. 145-150 min: 99 % B and equilibrate for 10 min at starting conditions. The nano-LC was connected to an LTQ ion trap-Orbitrap XL mass spectrometer (Thermo Fisher, Germany) and MS spectra (m/z 300-1500) were acquired. Up to ten peptide precursors were selected for collision induced dissociation fragmentation. Runs were, aligned in Progenesis LC-MS (Non-Linear Dynamics V3.0) and peptides were quantified by MS intensity. MS/MS spectra were searched against the Ensembl Mouse-database using Mascot (Matrix Science V2.3.02, precursor mass tolerance 7 ppm, fragment tolerance 0.7 Da, enzyme trypsin, fixed modifications: carbamidomethylation (C), dynamic modifications: oxidation (M) deamidation (N.Q)). Peptide false discory rate was set to 2% by adjusting cut-off values for Mascot-score and p-value using the decoy database approach.

Transmission electron microscopy (TEM). Liver blocks (~1 mm^3) were fixed in 2.5 % glutaraldehyde in 0.1 M sodium-cacodylate buffer pH 7.4 (Science Services, Germany), postfixed in 2 % aqueous osmium-tetraoxide, dehydrated in gradual ethanol (30–100 %) and propylene oxide, embedded in Epon (Merck, Germany) and cured 24 hours at 60 °C. Semi-thin sections were cut and stained with toluidine blue. Ultrathin 50 nm sections were collected onto 200 mesh copper grids, stained with uranyl acetate and lead citrate before TEM examination (Zeiss Libra 120Plus, Carl Zeiss NTS, Germany). Pictures were acquired using a slow-scan CCD-camera and iTEM software (Olympus Soft Imaging Solutions, Germany). In each individual liver ten periportal and ten perivenous images from different hepatocyte areas were morphometrically analyzed by hand using AxioVision Software (Carl Zeiss Microscopy, Germany). In each image we calculated the number of mitochondria and the mitochondrial volume occupying the predefined hepatocyte volume. The mean of each parameter obtained from the same liver was considered an n=1 and used to calculate the mean of each intervention group. Mitochondria <0.02 μm^3 were considered small, 0.02-0.07 μm^3 medium, and >0.07 μm^3 large.

Statistical analysis and data visualisation. We performed ANOVA's (Bonferroni post-hoc test) or t-tests and compared data from 7, 14, and 21 days HF-fed with pooled data from LF-fed, litter-matched controls. Exclusively for proteomics, individual LF control groups were compared with the respective age-matched HF groups, a Benjamini-Hochberg multiple testing correction was performed and a false discovery rate (FDR) <20% (HFd7, REC) or <10 % (HFd14, HFd21) was considered significant. Assessment of longitudinal alterations in protein signatures (except SLC25A12 and SLC25A3 in **Figure 4B**) was based on a set of 378 proteins, presenting the protein overlap between all groups. Enrichment analyzes, based on a custom liver-specific background dataset comprising 6212 proteins (**Supplemental Table 3**),

and protein networks were generated with STRING [24]. VENN diagrams were generated on the VENNY website [25] and heatmaps with MeV [26].

RESULTS

Development of HF-induced hepatosteatosis and hepatic insulin resistance. During a 21-day HF-challenge, mice progressively increased whole body fat content and visceral adipose mass (**Table 1**). Compared to the LF group, 7 days HF-exposure increased liver TAG concentrations ~8-fold (**Figure 1A**), liver mass ~1.2-fold (**Figure 1B**), and plasma alanine transaminase concentrations ~1.4-fold (**Table 1**), the latter suggesting modest hepatocellular injury. Extending HF-intervention from 7 to 21 days paradoxically reduced the degree of hepatosteatosis, however the marked increase in the liver's Met-SO/Met ratio compared to LF mice indicated oxidative stress (**Figure 1C**). Male C3HeB/FeJ mice maintained normoglycemia during HF-exposure (**Table 1**) but at the same time displayed ~2.9-fold higher plasma insulin concentrations on day 21 than LF mice suggesting insulin resistance (**Table 1**). To characterize HF-mediated alterations in insulin sensitivity *in vivo* we performed euglycemic-hyperinsulinemic clamps. Infusion of insulin raised plasma insulin concentrations from baseline levels on a comparable scale in all groups (**Figure 1D**). Furthermore, comparable blood glucose concentrations (**Figure 1E**) and plasma specific activities (**Figure 1F**) were achieved in all groups of mice during the final 30 minutes of the glucose-clamp. Mice treated with HF for 7 days maintained whole-body insulin sensitivity, whereas mice fed a HF for 14 days developed insulin resistance outlined by markedly reduced GIRs compared to LF mice (**Figure 1G**). Whole-body insulin resistance was further aggravated by extending HF-exposure to 21 days (**Figure 1G**). Basal endogenous glucose production rates ($EndoR_a$, **Figure 1H**) were similar in all groups, however insulin's ability to suppress the $EndoR_a$ tended to be decreased after 14 days and was significantly reduced after 21 days of HF feeding compared to LF mice (**Figure 1H**). Compared to basal, insulin administration markedly increased pAKT protein relative to total AKT protein in LF and 7 days HF-treated mice, whereas this response was attenuated in 21 days HF treated mice (**Figure 1I**).

HF-induced alterations in lipid membrane constituents in liver during developing hepatic insulin resistance. Next we assessed HF-mediated alterations of membrane-associated lipid metabolites in liver during developing hepatic insulin resistance. Seven days HF-intervention resulted in comprehensive lipid profile adaptations in insulin-sensitive livers (**Figure 2 A, B** first column). Seven, 14, and 21 days exposure to a HF diet rich in polyunsaturated fatty acids caused a marked ~3.0-, ~6.1-, and ~3.0-fold increase of polyunsaturated (**Figure 2C** left panel) and ~2.0-, ~2.5-, and ~1.6-fold increase of monounsaturated acyl-carnitines (**Figure 2C** middle panel). A pronounced ~1.4-fold increase in total hepatic diacylglycerol species containing at least one unsaturated fatty acid was already evident after 7 days HF exposure compared to LF animals (**Figure 2D,** left and middle panel). In addition, the abundance of total saturated acyl-carnitine species, total monounsaturated and saturated diacylglycerophosphocholines (**Figure 2E,** middle and left panel), total polyunsaturated and saturated glycerophosphocholines (**Figure 2F,** left and right panel), total saturated lysophosphatidylcholines (**Figure 2G,** right panel) and total hydroxylated or non-hydroxylated sphingolipids (**Figure 2H,** right panel) decreased significantly in livers after 7 days HF-exposure compared to the LF group. The transition stage between normal and marked hepatic insulin resistance at HF day 14, was associated with the most pronounced alterations in hepatic acyl-carnitines compared to 7 days HF mice (**Figure 2C** all panels). Fully developed hepatic insulin resistance induced by 21 days HF exposure, was paralleled by a relative drop in total poly- and monounsaturated acyl-carnitines (**Figure 2B** left and middle panel), but a relative increase in total monounsaturated diacylglycerophosphocholines (**Figure 2E** middle panel) and lysophosphatidylcholines (**Figure 2G** middle panel) in liver when compared to livers of modestly insulin resistant, 14 days HF treated mice. The data for all individual lipid species are provided in **Supplemental Table 1** and **2**.

HF-induced alterations in signatures of membrane-associated proteins in liver during developing hepatic insulin resistance. We determined whether changes in membrane lipids were paralleled by alterations of membrane-associated protein signatures during developing insulin resistance in liver. Among the 378 proteins identified in all experimental groups, 62 were significantly altered in abundance in liver after 7 days HF-exposure compared to LF animals. We detected the highest number of significantly differentially regulated membrane-associated proteins (159) in the transition stage from normal to impaired hepatic insulin sensitivity (HF day 14) and this number only modestly declined to 125 proteins once pronounced hepatic insulin resistance established (HF day 21; **Figure 3A**). Membrane fractions obtained from pre-insulin resistant livers (HF day 7) expressed the highest proportion of significantly upregulated membrane-associated proteins (71% of 62, **Figure 3B**) compared to the LF group. In contrast, the onset of mild (57% of 159) and marked (77 % of 125) HF-induced hepatic insulin resistance was paralleled by an increase in the proportion of markedly less abundant proteins (**Figure 3B**).

Compared to other cell types, liver cells are rich in mitochondria. To minimize an organ-specific bias we performed protein enrichment analyses based on a customized 6212 protein-background set constructed from the most comprehensive published mouse liver proteome-dataset [27] and our collected liver proteins (**Supplemental Table 3**). GO term analysis – based on the significantly differentially regulated proteins in HF- *versus* LF-treated mice – indicated a pronounced enrichment of e.g. the terms mitochondrial membrane, respiratory chain, or oxidative phosphorylation during developing hepatic insulin resistance (14 and 21 days HF; **Supplemental Table 3**). We visualized longitudinal changes in the network structures of down- (**Figure 3C**) and upregulated (**Figure 3D**) mitochondria-associated proteins during HF-intervention (see **Supplemental Table 3** for higher resolution images). Even though modest prior to the onset of hepatic insulin resistance (HF day 7), the abundance of approximately two thirds of the detected complex I, II, III, IV, and V

respiratory chain proteins – integral components of the inner mitochondrial membrane – tended to decrease (**Figure 4A**). Similar changes were observed for the majority of solute carrier family 25 members (**Figure 4B**), involved in the mitochondrial shuttling of adenine nucleotides (SLC25A13, SLC25A5), citrate (SLC25A1), oxoglutarate (SLC25A11), dicarboxylate (SLC25A10), ornithine (SLC25A15), carnitine/acyl-carnitine (SLC25A20), aspartate/glutamate (SLC25A12), or phosphate (SLC25A23). First signs of hepatic insulin resistance (HF day 14) were paralleled by a significantly lower abundance of most inner mitochondrial membrane constituents compared to LF-fed controls (**Figure 4A and B**). The expression of three voltage-dependent anion-selective channel (VDAC) family members (**Figure 4C**), associated with the outer mitochondrial membrane, tended to decrease within 14 days HF-intervention but significantly decreased when the HF-intervention was continued until day 21. Finally, the pronounced HF-induced alterations in hepatic mitochondria-related protein signatures, evident after 14 days HF-exposure, were completely reversible by switching mice back to a LF for 7 days (**Figure 4A-C**).

Ultrastructural changes in mitochondria during HF-mediated insulin resistance in liver.

We performed quantitative morphological analyzes to determine whether changes in the abundance of mitochondrial proteins during developing hepatic insulin resistance were attributable to changes in mitochondrial volume. Mitochondria of LF mice appeared as typical liver mitochondria, round or elongated in shape, with tubular cristae and a few electron dense granules in the mitochondrial matrix (**Figure 5A**, left panel). However, they strongly varied in size and a great amount had a size <0.01 μm^3. Mitochondria of mice exposed to HF for 7 days exhibited almost no pathological alterations. Only single mitochondria showed modest alterations such as fractures of the outer mitochondrial membrane (**Figure 5A**, arrow in middle panel). However, after 21 days HF exposure, numerous mitochondria appeared with an atypical electron-light mitochondrial matrix containing coiled membrane structures

(**Figure 5A**, asterisk in right panel), partially broken outer membranes and an exvaginated inner mitochondrial membrane (**Figure 5A**, arrow in right panel). Besides ultrastructural features, neither the mitochondrial number nor the mitochondrial volume (**Figure 5B**) in periportal and perivenous hepatocytes was altered by HF feeding. Confirming visual observations, a tendency towards a decrease in the area occupied by small mitochondria related to total mitochondrial area was observed in HF- compared to LF-fed mice (**Figure 5C**).

DISCUSSION

Insulin resistance is a growing global phenomenon predisposing to cardiovascular disease and type 2 diabetes mellitus. To comprehensively assess longitudinal alterations in liver membrane components during HF-induced hepatic insulin resistance we combined t-metabolomics and proteomics analyses with state-of-the-art phenotyping technologies of glucose metabolism.

Hepatosteatosis correlates with impaired hepatic insulin action; nevertheless it is debated whether insulin resistance or excess hepatic TAG concentrations develop first [28]. In our mouse model the hepatocellular TAG content increased more than eight-fold within seven days HF exposure, however hepatic insulin sensitivity remained normal. Hepatic insulin resistance developed, but was paralleled by a relative decline in the hepatocellular lipid content. In support of earlier findings in mice [7] we conclude that excess hepatic TAG accumulation *per se* does not abrogate hepatic insulin action. Based on the temporal fluctuations in hepatic TAG concentrations under HF-exposure it would be of particular value to investigate the secretory capacity of the liver regarding lipoproteins in more detail in the future.

The composition, overall intracellular availability, and subcellular distribution of glycerophospholipids, sphingolipids, diacylglycerols, and ceramides has been implicated in lipotoxicity-associated liver damage [29] and the pathogenesis of hepatic insulin resistance [6,12,28,30,31]. Prior to and throughout development of HF-mediated hepatic insulin resistance we observed comprehensive changes in membrane lipid signatures, which – besides affecting signal transduction cascades – likely modulate the physical properties and the topology of cellular membranes. For example the fluidity of synthetic lipid bilayers is determined by the composition of membrane lipids [13] what has been involved in the pathophysiology of metabolic disorders. A close correlation between the relative proportion of long-chain omega-3 polyunsaturated fatty acids in phospholipid and insulin action in red

quadriceps muscle has been outlined earlier [32]. Based on our data we propose a similar hypothesis in liver and in the following discuss both, evidence and potential mechanisms of how HF-induced alterations in membrane lipid signatures might contribute to the development of insulin resistance.

Acyl-carnitines link fatty acid and glucose metabolism, are crucial for cell function and survival, for mitochondrial fatty acyl-CoA thioester import, or acyl-group export from mitochondria and peroxisomes [33]. In addition, carnitine O-acyl derivatives modulate membrane fluidity *via* direct interactions with cell membranes, influence ion channel functions as well as membrane stability in cardiac tissue [34]. When we exposed mice to a diet rich in long-chain fatty acids they initially accumulated long-chain poly- and monounsaturated acyl-carnitines in liver followed by a relative decline. Due to their multiple functions and as long-chain acyl-carnitines bind to phospholipid bilayers and appear to almost completely reside in the membrane phase [35], such modifications might alter physical membrane properties and contribute to the development of insulin resistance in liver.

The outer and inner monolayer of lipid bilayers is thought to present a striking lipid asymmetry; whereas the outer membrane monolayer of e.g. human erythrocytes predominantly contains phosphatidylcholines and sphingomyelins, the inner monolayer is rather enriched in phosphatidylserines and phosphatidylethanolamines [13]. Lipid asymmetry is functionally important as many cytosolic proteins only bind to specific lipid head groups presented by the cytosolic face of the lipid monolayer, e.g. protein kinase C to regions rich in negatively charged phosphatidylserine [13]. A relationship between the composition of membrane structural phospholipids and insulin sensitivity was outlined in skeletal muscle of animal models and humans [32,36,37]. In skeletal muscle, diet-induced alterations in phospholipid moiety were speculated to influence insulin action in part by altering membrane fluidity [32]. In rat adipocytes, dietary fat-mediated modifications in the membrane

phospholipid composition increased the fluidity of the plasma membrane lipid bilayer with the degree of phospholipid-incorporated polyunsaturated fatty acids [38].

Noteworthy, phospholipid signatures in this study do not accurately reflect membrane lipids as they were measured in whole liver homogenates. We chose to extract lipids from immediately freeze-clamped livers rather than from membrane extracts following an additional enrichment procedure as thereby we likely conserved low-abundant, rapidly metabolized, and degradation susceptible phospholipid signatures more efficiently. Presumably the analysed phospholipids predominantly reside in cellular membranes rather than in extra-membranous compartments as according to their amphipatic nature they preferentially assemble into bilayers in aquatic (e.g. cytosolic) environments.

Taken together, our data outline comprehensive changes in unsaturated and saturated moieties of predominantly membrane-associated phospholipids, DAGs, and acyl-carnitines in mouse liver in response to HF-exposure. Given that the spontaneous curvature of a lipid depends on both, length and saturation of its incorporated fatty acids [39], HF-induced temporal changes in the degree of saturation and chain length of structural membrane lipids suggest dynamic alterations in physical membrane bilayer properties in liver. These might impact on the physiology of cells and those of cell organelles, on cellular energy metabolism, and thereby contribute to hepatic insulin resistance. Thus it will be an important future asset for the development of effective prevention and treatment strategies for type 2 diabetes and NAFLD to further elucidate initial mechanisms by which bioactive lipid metabolites interfere with hepatic insulin action.

In humans and animal models mitochondrial adaptations, such as epigenetic modifications of mitochondrial DNA, alterations in mitochondrial DNA content, respiratory chain complex activity, or mitochondrial beta-oxidation capacity in liver, have been linked to the development of hepatosteatosis, hepatic insulin resistance, and type 2 diabetes [40-44]. Also ultrastructural mitochondrial changes, their superior organisation, and plasticity seem to

play pivotal roles in the development of insulin resistance [45-47]. Hepatocytes contain numerous, double membrane-bounded mitochondria and the organelles occupied approximately 18% of the cell volume in our mouse model (**Figure 5B**). The outer and inner mitochondrial membranes perform different functions and are characterized by distinct lipid and protein compositions [48]. In mice, HF-induced development of hepatic insulin resistance was accompanied by a gradual decrease in the abundance of many mitochondrial inner and outer membrane proteins involved in oxidative phosphorylation or substrate shuttling, what was not attributable to a decrease in the mitochondrial area in hepatocytes. Mitochondrial energetics significantly depends on the organelles complex internal architecture. Cristae, inner mitochondrial membrane invaginations, are sites of oxidative phosphorylation and ATP synthesis catalyzed by the mitochondrial ATP synthase. The enzyme is composed of two linked complexes. One is termed the soluble catalytic core F_1, the second is the membrane-spanning, proton channel comprising F_o complex which is composed of nine subunits (A, B, C, D, E, F, G, F6, and 8). ATP synthase seems crucial for proper cristae morphogenesis [49,50] and assembles into dimers in cristae regions with a high membrane curvature [50-52]. In our study HF-exposure markedly decreased the abundance of the mitochondrial ATP synthase F_o complex subunits ATP5L (subunit G), ATP5K (subunit E), ATP5J (subunit F6), and ATP5H (subunit D) in liver. In mutant yeast cells the disruption in the ATP synthase F_o subunit *e* or *g* genes altered ATP synthase dimerization and caused defects in cristae architecture and so called 'onion'-like structures [53,54]. Thus, the decrease in the abundance of ATP synthase subunit E or G proteins in our model may impact dimerization and be connected to the ultrastructural changes in the inner mitochondrial membrane architecture.

The volume-constraining outer mitochondrial membrane serves as an interface between the cytosol and mitochondria and establishes contact sites to cristae. VDACs are master regulators of the metabolite flux between the cytosol and the outer mitochondrial membrane [55]. In mice, VDAC1 deficiency leads to defects in respiratory complex activities

in striated muscles and VDAC3-deficiency to alterations in complex IV in heart paralleled by mitochondrial structural abnormalities [56]. VDAC1 seems capable of interacting with hexokinase [57], the latter implicated in reducing mitochondrial ROS generation through an ADP-recycling mechanism. Outlining a role for VDAC1 in the development of HF-mediated hepatic insulin resistance in mice, deterioration of hepatic insulin action was paralleled by a significant reduction in the abundance of VDAC1 protein, an increase in oxidative stress and changes in mitochondrial architecture in liver.

Finally, HF-induced alterations in mitochondrial proteins of the inner and outer membrane were almost completely reversible within seven days upon treatment with a low fat diet. This suggests that diet and life-style interventions contribute to a rapid restoration of insulin sensitivity in liver, at least at an early stage of hepatic insulin resistance. It will be of significance to further explore whether a longer HF-exposure extends the recovery of mitochondrial membrane proteins back to baseline or results in irreversible alterations and how it affects membrane associated lipid profiles.

The KEGG pathway of human NAFLD (hsa04932) implicates alterations in mitochondrial oxidative phosphorylation in the pathophysiology of the disease. However, it will be important to translate the alterations in mitochondrial inner and outer membranes in mice to humans with clinical manifestation of hepatosteatosis, as to our knowledge no studies specifically explored the human liver membrane proteome yet.

CONCLUSIONS

Diet-derived lipids modified signatures of membrane-constituting lipid classes such as the proportions of saturated and unsaturated long-chain acyl-carnitines, membrane-associated diacylglycerols, glycerophosphocholines, and glycerophospholipids in livers of mice. We assume this affects mitochondrial membrane topology and organelle physiology in liver. Therefore, it will be valuable to examine whether changes in the membrane lipid composition indeed interfere with the distribution of proteins in mitochondrial membranes or alter

mitochondrial cristae formation, which would explain the observed decrease in the abundance of inner and outer mitochondrial membrane-associated proteins. It is tempting to speculate that persistent and comprehensive reductions of inner- and outer mitochondrial membrane-associated respiratory chain and substrate carrier proteins impede mitochondrial bioenergetics, substrate exchange with extramitochondrial compartments, provoke oxidative stress, induce mitochondrial damage, and thereby play a role in the development of hepatic insulin resistance.

ACKNOWLEDGEMENT

We thank E. Holupirek, A.E. Schwarz, V. Gailus-Durner, H. Fuchs, and all animal caretakers in the GMC who contributed expert technical and organisational help with mouse phenotyping and care. We greatly appreciate the valuable scientific contributions of M. Horsch, A. Franko, and P. Huypens. The authors are very grateful to G.I. Shulman, M. Kahn, and G.W. Cline who measured DAGs, K. Suhre for providing expertise with metabolomics and biomathematical analyses, C. Prehn, W. Römisch-Margl, J. Scarpa, and K. Sckell for metabolomics measurements, the latter performed at the Helmholtz Zentrum München, Genome Analysis Center, Metabolomics Core Facility.

This work was funded by grants from the German Federal Ministry of Education and Research (BMBF) to the German Center for Diabetes Research (DZD e.V.), from the BMBF (SysMBo 0315494A) and from the National Institutes of Health (U24 DK-059635).

CONFLICT OF INTEREST

No potential conflict of interest relevant to this article was declared.

REFERENCES

1. Pappachan JM, Antonio FA, Edavalath M, Mukherjee A (2014) Non-alcoholic fatty liver disease: a diabetologist's perspective. Endocrine 45: 344-353.
2. Samuel VT, Shulman GI (2012) Mechanisms for insulin resistance: common threads and missing links. Cell 148: 852-871.
3. Ikai E, Ishizaki M, Suzuki Y, Ishida M, Noborizaka Y, et al. (1995) Association between hepatic steatosis, insulin resistance and hyperinsulinaemia as related to hypertension in alcohol consumers and obese people. J Hum Hypertens 9: 101-105.
4. Perry RJ, Samuel VT, Petersen KF, Shulman GI (2014) The role of hepatic lipids in hepatic insulin resistance and type 2 diabetes. Nature 510: 84-91.
5. Holland WL, Knotts TA, Chavez JA, Wang LP, Hoehn KL, et al. (2007) Lipid mediators of insulin resistance. Nutr Rev 65: S39-46.
6. Larsen PJ, Tennagels N (2014) On ceramides, other sphingolipids and impaired glucose homeostasis. Mol Metab 3: 252-260.
7. Neschen S, Morino K, Dong J, Wang-Fischer Y, Cline GW, et al. (2007) n-3 Fatty acids preserve insulin sensitivity in vivo in a peroxisome proliferator-activated receptor-alpha-dependent manner. Diabetes 56: 1034-1041.
8. Neschen S, Morino K, Hammond LE, Zhang D, Liu Z-X, et al. (2005) Prevention of hepatic steatosis and hepatic insulin resistance in mitochondrial acyl-CoA:glycerol-sn-3-phosphate acyltransferase 1 knockout mice. Cell Metabolism 2: 55-65.
9. Samuel VT, Liu Z-X, Qu X, Elder BD, Bilz S, et al. (2004) Mechanism of Hepatic Insulin Resistance in Non-alcoholic Fatty Liver Disease. Journal of Biological Chemistry 279: 32345-32353.
10. Jump DB, Botolin D, Wang Y, Xu J, Christian B, et al. (2005) Fatty acid regulation of hepatic gene transcription. J Nutr 135: 2503-2506.
11. Fayyaz S, Japtok L, Kleuser B (2014) Divergent role of sphingosine 1-phosphate on insulin resistance. Cell Physiol Biochem 34: 134-147.
12. Kumashiro N, Erion DM, Zhang D, Kahn M, Beddow SA, et al. (2011) Cellular mechanism of insulin resistance in nonalcoholic fatty liver disease. Proc Natl Acad Sci U S A 108: 16381-16385.
13. Alberts B JA, Lewis J, et al. (2002) The Lipid Bilayer. Molecular Biology of the Cell. 4th edition. New York: Garland Science; Available from: http://www.ncbi.nlm.nih.gov/books/NBK26871/
14. Haag M, Dippenaar NG (2005) Dietary fats, fatty acids and insulin resistance: short review of a multifaceted connection. Med Sci Monit 11: Ra359-367.
15. Hulbert AJ, Turner N, Storlien LH, Else PL (2005) Dietary fats and membrane function: implications for metabolism and disease. Biol Rev Camb Philos Soc 80: 155-169.
16. Lee AG (1991) Lipids and their effects on membrane proteins: evidence against a role for fluidity. Prog Lipid Res 30: 323-348.
17. Kahle M, Horsch M, Fridrich B, Seelig A, Schultheiss J, et al. (2013) Phenotypic comparison of common mouse strains developing high-fat diet-induced hepatosteatosis. Mol Metab 2: 435-446.
18. Neschen S, Scheerer M, Seelig A, Huypens P, Schultheiss J, et al. (2014) Metformin supports the antidiabetic effect of a sodium glucose cotransporter 2 (SGLT2) inhibitor by suppressing endogenous glucose production in diabetic mice. Diabetes.
19. Zukunft S, Sorgenfrei M, Prehn C, Möller G, Adamski J (2013) Targeted Metabolomics of Dried Blood Spot Extracts. Chromatographia 76: 1295-1305.
20. Bauer C, Melamed ML, Hostetter TH (2008) Staging of chronic kidney disease: time for a course correction. J Am Soc Nephrol 19: 844-846.

21. Yu C, Chen Y, Cline GW, Zhang D, Zong H, et al. (2002) Mechanism by which fatty acids inhibit insulin activation of insulin receptor substrate-1 (IRS-1)-associated phosphatidylinositol 3-kinase activity in muscle. J Biol Chem 277: 50230-50236.
22. Nagaraj N, Lu A, Mann M, Wisniewski JR (2008) Detergent-based but gel-free method allows identification of several hundred membrane proteins in single LC-MS runs. J Proteome Res 7: 5028-5032.
23. Hauck SM, Dietter J, Kramer RL, Hofmaier F, Zipplies JK, et al. (2010) Deciphering membrane-associated molecular processes in target tissue of autoimmune uveitis by label-free quantitative mass spectrometry. Mol Cell Proteomics 9: 2292-2305.
24. Franceschini A, Szklarczyk D, Frankild S, Kuhn M, Simonovic M, et al. (2013) STRING v9.1: protein-protein interaction networks, with increased coverage and integration. Nucleic Acids Res 41: D808-815.
25. JC O (2007) VENNY. An interactive tool for comparing lists with Venn Diagrams. BioinfoGP, CNB-CSIC Online Access
26. Howe E HK, Nair S, Schlauch D, Sinha R, Quackenbush J (2010) MeV: MultiExperiment Viewer. In Biomedical Informatics for Cancer Research Ochs MF, Casagrande JT, Davuluri RV, Eds, Springer US, p267-277.
27. Lai KK, Kolippakkam D, Beretta L (2008) Comprehensive and quantitative proteome profiling of the mouse liver and plasma. Hepatology 47: 1043-1051.
28. Nagle CA, Klett EL, Coleman RA (2009) Hepatic triacylglycerol accumulation and insulin resistance. J Lipid Res 50 Suppl: S74-79.
29. Neuschwander-Tetri BA (2010) Hepatic lipotoxicity and the pathogenesis of nonalcoholic steatohepatitis: the central role of nontriglyceride fatty acid metabolites. Hepatology 52: 774-788.
30. Russo SB, Ross JS, Cowart LA (2013) Sphingolipids in obesity, type 2 diabetes, and metabolic disease. Handb Exp Pharmacol: 373-401.
31. Samuel VT, Petersen KF, Shulman GI (2010) Lipid-induced insulin resistance: unravelling the mechanism. Lancet 375: 2267-2277.
32. Storlien LH, Jenkins AB, Chisholm DJ, Pascoe WS, Khouri S, et al. (1991) Influence of dietary fat composition on development of insulin resistance in rats. Relationship to muscle triglyceride and omega-3 fatty acids in muscle phospholipid. Diabetes 40: 280-289.
33. Zammit VA, Ramsay RR, Bonomini M, Arduini A (2009) Carnitine, mitochondrial function and therapy. Adv Drug Deliv Rev 61: 1353-1362.
34. Fritz IB, Arrigoni-Martelli E (1993) Sites of action of carnitine and its derivatives on the cardiovascular system: interactions with membranes. Trends Pharmacol Sci 14: 355-360.
35. Ho JK, Duclos RI, Jr., Hamilton JA (2002) Interactions of acyl carnitines with model membranes: a (13)C-NMR study. J Lipid Res 43: 1429-1439.
36. Borkman M, Storlien LH, Pan DA, Jenkins AB, Chisholm DJ, et al. (1993) The relation between insulin sensitivity and the fatty-acid composition of skeletal-muscle phospholipids. N Engl J Med 328: 238-244.
37. Pan DA, Lillioja S, Milner MR, Kriketos AD, Baur LA, et al. (1995) Skeletal muscle membrane lipid composition is related to adiposity and insulin action. J Clin Invest 96: 2802-2808.
38. Parrish CC, Myher JJ, Kuksis A, Angel A (1997) Lipid structure of rat adipocyte plasma membranes following dietary lard and fish oil. Biochim Biophys Acta 1323: 253-262.
39. Szule JA, Fuller NL, Rand RP (2002) The effects of acyl chain length and saturation of diacylglycerols and phosphatidylcholines on membrane monolayer curvature. Biophys J 83: 977-984.

40. Begriche K, Massart J, Robin MA, Bonnet F, Fromenty B (2013) Mitochondrial adaptations and dysfunctions in nonalcoholic fatty liver disease. Hepatology 58: 1497-1507.
41. Caldwell SH, Swerdlow RH, Khan EM, Iezzoni JC, Hespenheide EE, et al. (1999) Mitochondrial abnormalities in non-alcoholic steatohepatitis. J Hepatol 31: 430-434.
42. Pessayre D (2007) Role of mitochondria in non-alcoholic fatty liver disease. J Gastroenterol Hepatol 22 Suppl 1: S20-27.
43. Pirola CJ, Gianotti TF, Burgueno AL, Rey-Funes M, Loidl CF, et al. (2013) Epigenetic modification of liver mitochondrial DNA is associated with histological severity of nonalcoholic fatty liver disease. Gut 62: 1356-1363.
44. Wei Y, Rector RS, Thyfault JP, Ibdah JA (2008) Nonalcoholic fatty liver disease and mitochondrial dysfunction. World J Gastroenterol 14: 193-199.
45. Kim J-a, Wei Y, Sowers JR (2008) Role of Mitochondrial Dysfunction in Insulin Resistance. Circulation Research 102: 401-414.
46. Lieber CS, Leo MA, Mak KM, Xu Y, Cao Q, et al. (2004) Model of nonalcoholic steatohepatitis. The American Journal of Clinical Nutrition 79: 502-509.
47. Rector RS, Thyfault JP, Uptergrove GM, Morris EM, Naples SP, et al. (2010) Mitochondrial dysfunction precedes insulin resistance and hepatic steatosis and contributes to the natural history of non-alcoholic fatty liver disease in an obese rodent model. J Hepatol 52: 727-736.
48. Vance JE (2014) MAM (mitochondria-associated membranes) in mammalian cells: lipids and beyond. Biochim Biophys Acta 1841: 595-609.
49. Holme E, Greter J, Jacobson CE, Larsson NG, Lindstedt S, et al. (1992) Mitochondrial ATP-synthase deficiency in a child with 3-methylglutaconic aciduria. Pediatr Res 32: 731-735.
50. Jimenez L, Laporte D, Duvezin-Caubet S, Courtout F, Sagot I (2014) Mitochondrial ATP synthases cluster as discrete domains that reorganize with the cellular demand for oxidative phosphorylation. J Cell Sci 127: 719-726.
51. Buzhynskyy N, Sens P, Prima V, Sturgis JN, Scheuring S (2007) Rows of ATP synthase dimers in native mitochondrial inner membranes. Biophys J 93: 2870-2876.
52. Habersetzer J, Ziani W, Larrieu I, Stines-Chaumeil C, Giraud MF, et al. (2013) ATP synthase oligomerization: from the enzyme models to the mitochondrial morphology. Int J Biochem Cell Biol 45: 99-105.
53. Paumard P, Vaillier J, Coulary B, Schaeffer J, Soubannier V, et al. (2002) The ATP synthase is involved in generating mitochondrial cristae morphology. Embo j 21: 221-230.
54. Arselin G, Gandar JC, Guerin B, Velours J (1991) Isolation and complete amino acid sequence of the mitochondrial ATP synthase epsilon-subunit of the yeast Saccharomyces cerevisiae. J Biol Chem 266: 723-727.
55. Colombini M (2012) VDAC structure, selectivity, and dynamics. Biochim Biophys Acta 1818: 1457-1465.
56. Anflous-Pharayra K, Lee N, Armstrong DL, Craigen WJ (2011) VDAC3 has differing mitochondrial functions in two types of striated muscles. Biochim Biophys Acta 1807: 150-156.
57. Anflous-Pharayra K, Cai ZJ, Craigen WJ (2007) VDAC1 serves as a mitochondrial binding site for hexokinase in oxidative muscles. Biochim Biophys Acta 1767: 136-142.

FIGURE LEGENDS

Figure 1. **Induction of HF-mediated hepatic steatosis and insulin resistance.** Male mice were exposed to HF or LF (pooled) for 7, 14, or 21 days. The liver parameters **A)** liver triacylglycerol concentrations, **B)** terminal liver mass, and **C)** liver ratio of methionine-SO and methionine (oxidative stress indicator) were assessed in random-fed mice (n=6-24). Euglycemic-hyperinsulinemic clamps were performed in conscious, 17-hour fasting (= basal condition, B) mice. **D)** Plasma insulin concentrations in the B condition and in the clamp 'steady state' during insulin-stimulation (IS). The following parameters were calculated for 10 minute periods in the clamp 'steady state'. **E)** Blood glucose concentration. **F)** Plasma specific activity. **G)** Glucose infusion rate. **H)** Endogenous glucose appearance rates ($EndoR_a$, B and IS), **I)** Liver ratio of pAKT and total AKT protein (t-test comparing B and IS in each group, n=4-15/group). Data are means±SEM. n=8-15/group. *p < 0.05; **p < 0.01; ***p < 0.001; ****p < 0.0001 *vs*. LF or *vs*. B (ANOVA, Bonferroni).

Figure 2. Liver lipid profiles during developing HF-mediated hepatic insulin resistance. *Via* t-metabolomics liver lipid profiles were assessed in random-fed male mice following exposure to HF or LF (pooled) for 7, 14, or 21 days. Heatmaps depict fold-change (log2) of individual **A)** short-, medium- and long-chain acyl-carnitine species or **B)** selected phospholipid species in each HF-group. Compared to the LF-group, an increase in the HF-fed groups is indicated in yellow and a decrease in blue. **C)** Total polyunsaturated (left, 4 species), monounsaturated (middle, 10 species) and saturated (right, 11 species) acyl-carnitine species. **D)** Total membrane-associated diacylglycerols with two (left, 4 species) or one (middle, 6 species) incorporated unsaturated fatty acid or two incorporated saturated fatty acids (right, 3 species). **E)** Total polyunsaturated (left, 31 species), monounsaturated (middle, 7 species) and saturated (right, 7 species) diacylglycerophosphocholines, **F)** Total

polyunsaturated (left, 19 species), monounsaturated (middle, 7 species) and saturated (right, 6 species) glycerophosphocholines, and **G)** Total polyunsaturated (left, 3 species), monounsaturated (middle, 4 species) and saturated (right, 8 species) lysophosphatidylcholines. **H)** Total hydroxylated (left, 5 species) or non-hydroxylated (right, 7 species) sphingomyelins. Data are means±SEM. n=6-24/group, except diacylglycerols n=6-9/group. *p < 0.05; **p < 0.01; ***p < 0.001; ****p < 0.0001 *vs*. LF (ANOVA, Bonferroni). Abbreviations: PC aa diacylglycerophosphocholine (lecitine); PC ae, glycerophosphocholine (plasmalogen); lysoPC, lysophosphatidylcholine (lysolecithine); SM, sphingolipid.

Figure 3. Liver membrane protein profiles during developing HF-mediated hepatic insulin resistance. *Via* quantitative proteomics liver membrane protein profiles were assessed in random-fed male mice following exposure to HF or LF for 7, 14, or 21 days. **A)** VENNY diagram depicts the overlap of significantly regulated membrane-associated proteins comparing a HF *versus* the respective LF group. **B)** Number of significantly up- and downregulated proteins. **C)** Up- and **D)** downregulated mitochondria-associated proteins were identified in a HF *versus* the respective LF group and used to generate networks. n=6-7/group. HFd7: FDR<20%, HFd14 and HFd21: FDR<10%.

Figure 4. Liver inner and outer mitochondria-membrane protein profiles during developing HF-mediated hepatic insulin resistance. *Via* quantitative proteomics liver membrane protein profiles were assessed in random-fed male mice following exposure to HF or LF for 7, 14, or 21 days or following 7 days recovery on LF after 14 d HF-exposure (REC) compared to LF-fed littermates. Heatmaps depict the fold-change in the abundance of inner mitochondrial membrane-associated **A)** respiratory chain complexes I-V and **B)** solute carrier proteins, and outer mitochondrial membrane-associated **C)** VDAC proteins. n=6-7/group. * Significantly regulated proteins in HF, REC *versus* LF group. HFd7: FDR<20%, HFd14 and

HFd21: FDR<10%. Abbreviations: RC I-V, respiratory chain complexes I-V; SLC, solute carrier family 25 member, N.d. not detected.

Figure 5. Ultrastructural and morphometric mitochondrial features in liver during development of HF-induced hepatic insulin resistance. EM-analyses were performed in liver sections obtained from random-fed male mice following exposure to LF or HF for 7 or 21 days. **A)** Mitochondria in hepatocytes of the HFd7 group depicted minor ultrastructural changes (arrow middle panel, third row) whereas those of animals in the HFd21 group contained numerous atypical mitochondria with 'onion-like' structures (* right panel second and third row). Morphometric analyses of EM liver sections outline the **B)** Percentages of periportal and perivenous hepatocyte volumina occupied by mitochondria and relative volumina of **C)** small-sized mitochondria (defined as <0.02 μm^3) related to total mitochondrial volume. Data are means±SEM. n=3-4/group (n=1 represents mean of 10 analyzed electron micrographs/area and animal, ANOVA, Bonferroni).

TABLE FOOTNOTE

Table 1. Phenotypic characterisation of mice developing HF-induced hepatic insulin resistance. Prior to the start of the experiment animals in the LF (n=28; pooled from 7, 14, or 21 days LF-fed mice) and HF groups (n=10/group) were litter- and body mass-matched. Plasma analyses were performed in samples obtained from random-fed mice between 9-11 am prior to and after 7, 14, or 21 days HF- or LF-feeding. Group sizes for mesenteric WAT mass (n=18, 9, 5, 5 for LF, HFd7, HFd14, HFd21), for plasma alanine aminotransferase and creatine kinase (n=24, 6, 8, 10 for LF, HFd7, HFd14, HFd21) and for plasma insulin (n=8 for HFd7) were lower due to plasma limitations. The lower section of the table depicts the Rate of glucose disappearance (Rd) estimated for 10 minute intervals during the final 30 minutes of the euglycemic-hyperinsulinemic clamps (n=9, 8, 9, 9 for LF, HFd7, HFd14, HFd21). Data are means±SEM.*p < 0.05; **p < 0.01; ***p < 0.001; ****p < 0.0001 *vs*. LF (ANOVA, Bonferroni).

SUPPLEMENTAL MATERIAL

Supplemental Table 1. Membrane-associated phospholipid signatures in livers during developing HF-induced hepatic insulin resistance. *Via* t-metabolomics lipid profiles were assessed in livers obtained from random-fed male mice following exposure to HF or LF (pooled) for 7, 14, or 21 days. The table depicts the concentrations of individual **A**) short-, medium- and long-chain carnitine acyl-esters and **B**) phospholipids in liver. Data are means±SEM. n=6-24/group. *p < 0.05; **p < 0.01; ***p < 0.001; ****p < 0.0001 *vs*. LF (ANOVA, Bonferroni). Abbreviations: PC aa diacylglycerophosphocholine (lecitine); PC ae, glycerophosphocholine (plasmalogen); lysoPC, lysophosphatidylcholine (lysolecithine); SM, sphingolipid.

Supplemental Table 2. Membrane-associated diacylglycerol signatures in livers during developing HF-induced hepatic insulin resistance. Liver membrane-associated diacylglycerol species were assessed in six-hour fasting, male mice following exposure to HF or LF (pooled) for 7, 14, or 21 days. Data are means±SEM. n=6-9/group. *p < 0.05; **p < 0.01; ***p < 0.001; ****p < 0.0001 *vs*. LF (ANOVA, Bonferroni).

Supplemental Table 3. GO-term analysis of significantly regulated liver proteins during developing HF-induced hepatic insulin resistance and 6212 protein background dataset *Via* quantitative proteomics liver membrane protein profiles were assessed in random-fed male mice. The tables depict results from GO-term analyses performed with proteins significantly differentially expressed in livers obtained from 7 (no enrichment), 14, or 21 days HF- *versus* LF-treated mice and to avoid an organ-specific bias based on a custom-made 6212 liver protein background dataset (provided). n=6-7/group. HFd7: FDR<20%, HFd14 and HFd21: FDR<10%.

Table 1. Phenotypic parameters during developing HF-induced hepatic insulin resistance. Measurements were conducted in random-fed mice between 9 and 11 am. Prior to the start of the experiment animals in the LF (n=28; pooled from 7, 14, or 21 days LF-fed mice) and HF groups (n=10 each) were litter- and body mass-matched. Group sizes for mesenteric WAT mass (n=18, 9, 5, and 5 for LF, HFd7, HFd14, and HFd21, respectively), for plasma alanine aminotransferase and creatine kinase (n=24, 6, 8, and 10 for LF, HFd7, HFd14, and HFd21, respectively) and for plasma insulin (n=8 for HFd7) were lower as not all parameters could be measured in each mouse. The table depicts the Rate of glucose disappearance (Rd) during the final 30 minutes of the glucose clamp (n=9, 8, 9, and 9 for LF, HFd7, HFd14, and HFd21, respectively). All data are given as means±SEM (ANOVA, Bonferroni). * p<0.05, p<0.01 ** p<0.001 *** p<0.0001 ****

Physiological parameters (random-fed)	LF	HF d7	HF d14	HF d21
Terminal body mass (g)	34.14 ± 0.45	38.15 ± 0.76***	38.46 ± 1.06***	40.90 ± 0.81****
Body mass gain (terminal-initial. g)	-0.08 ± 0.24	2.98 ± 0.39****	4.84 ± 0.40****	6.88 ± 0.67****
Terminal whole body fat mass (g)	9.30 ± 0.26	11.94 ± 0.49***	12.12 ± 0.73****	13.08 ± 0.46****
Body fat mass gain (terminal-initial. g)	0.15 ± 0.19	1.62 ± 0.25***	3.12 ± 0.41****	3.63 ± 0.27****
Epididymal white adipose tissue mass (g)	0.93 ± 0.04	1.50 ± 0.07****	1.51 ± 0.10****	1.66 ± 0.06****
Mesenteric white adipose tissue mass (g)	0.57 ± 0.03	0.95 ± 0.04****	0.97 ± 0.07****	1.14 ± 0.06****
Plasma alanine aminotransferase (U/l)	21.94 ± 1.65	31.45 ± 2.13*	26.36 ± 1.88	28.92 ± 3.09
Plasma creatine kinase (U/l)	42.50 ± 2.50	29.00 ± 2.67*	33.00 ± 2.51	36.20 ± 3.39
Plasma glucose (mmol/l)	11.49 ± 0.49	12.35 ± 0.59	14.52 ± 1.42	10.93 ± 0.60
Plasma insulin (pmol/l)	339.50 ± 76.47	867.60 ± 161.30	642.00 ± 167.10	976.90 ± 313.60*
Plasma triacylglycerol (mmol/l)	4.07 ± 0.27	1.96 ± 0.13***	2.62 ± 0.33*	2.76 ± 0.35*
Plasma non-esterified fatty acids (mmol/l)	0.71 ± 0.05	0.51 ± 0.05	0.60 ± 0.08	0.58 ± 0.06
Euglycemic-hyperinsulinemic clamps (~17-h fasting)				
Rd t90 [mmol/kg*min]	1.92 ± 0.14	1.75 ± 0.04	1.47 ± 0.11*	1.38 ± 0.08**
Rd t100 [mmol/kg*min]	1.86 ± 0.09	1.74 ± 0.07	1.52 ± 0.10	1.37 ± 0.08**
Rd t110 [mmol/kg*min]	1.83 ± 0.10	1.75 ± 0.09	1.50 ± 0.10	1.35 ± 0.09**
Rd t120 [mmol/kg*min]	1.86 ± 0.07	1.76 ± 0.16	1.53 ± 0.10	1.40 ± 0.09*

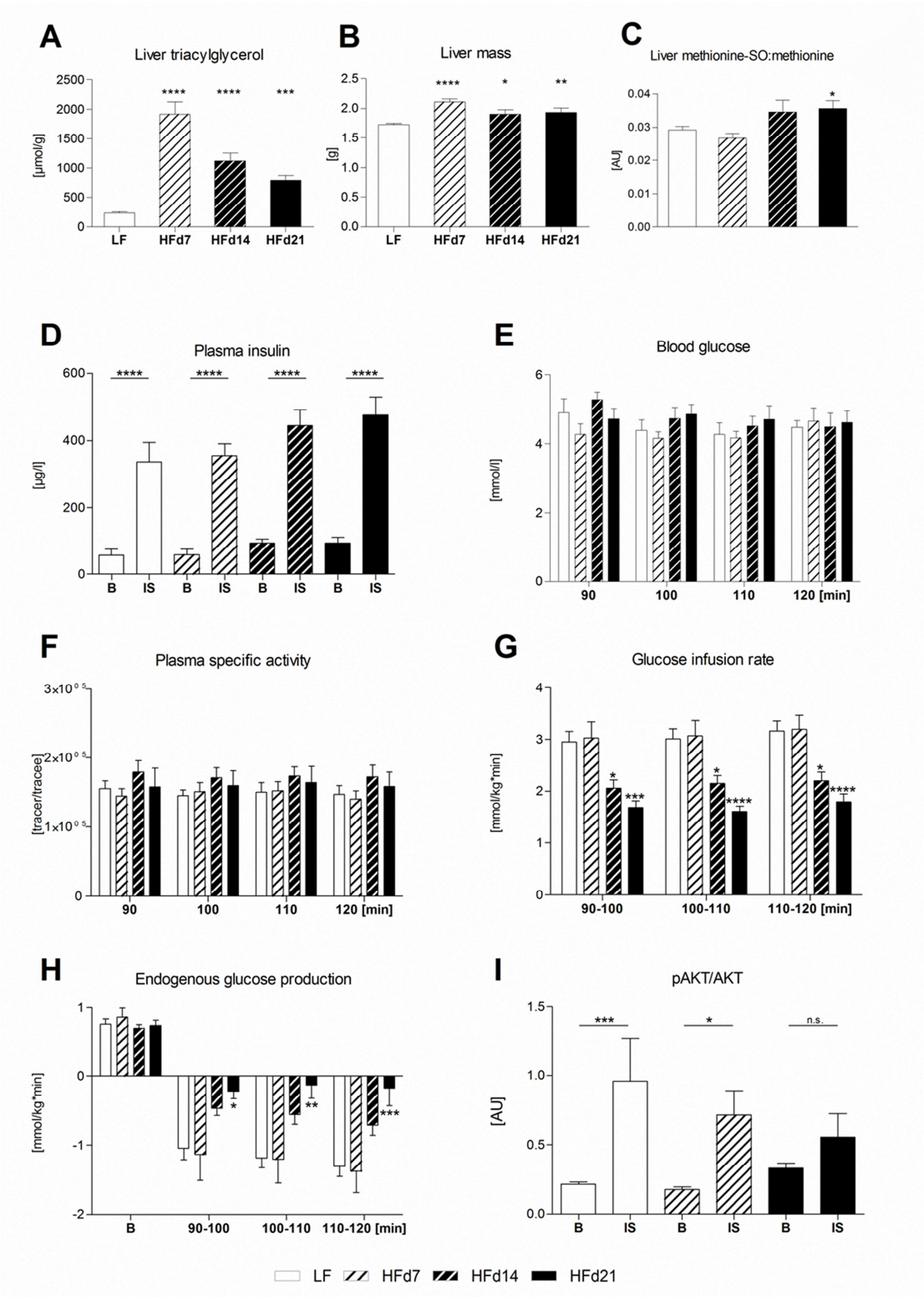
A
Liver triacylglycerol
[µmol/g]
2500
2000
1500
1000
500
0
****
****
***
LF
HFd7
HFd14
HFd21
B
Liver mass
[g]
2.5
2.0
1.5
1.0
0.5
0.0
****
*
**
LF
HFd7
HFd14
HFd21
C
Liver methionine-SO:methionine
[AU]
0.04
0.03
0.02
0.01
0.00
*
D
Plasma insulin
[µg/l]
600
400
200
0
****
****
****
****
B
IS
B
IS
B
IS
B
IS
E
Blood glucose
[mmol/l]
6
4
2
0
90
100
110
120 [min]
F
Plasma specific activity
[tracer/tracee]
3x10⁻⁵
2x10⁻⁵
1x10⁻⁵
0
90
100
110
120 [min]
G
Glucose infusion rate
[mmol/kg*min]
4
3
2
1
0
*
***
*
****
*
****
90-100
100-110
110-120 [min]
H
Endogenous glucose production
[mmol/kg*min]
1
0
-1
-2
*
**
***
B
90-100
100-110
110-120 [min]
I
pAKT/AKT
[AU]
1.5
1.0
0.5
0.0
***
*
n.s.
B
IS
B
IS
B
IS
LF
HFd7
HFd14
HFd21

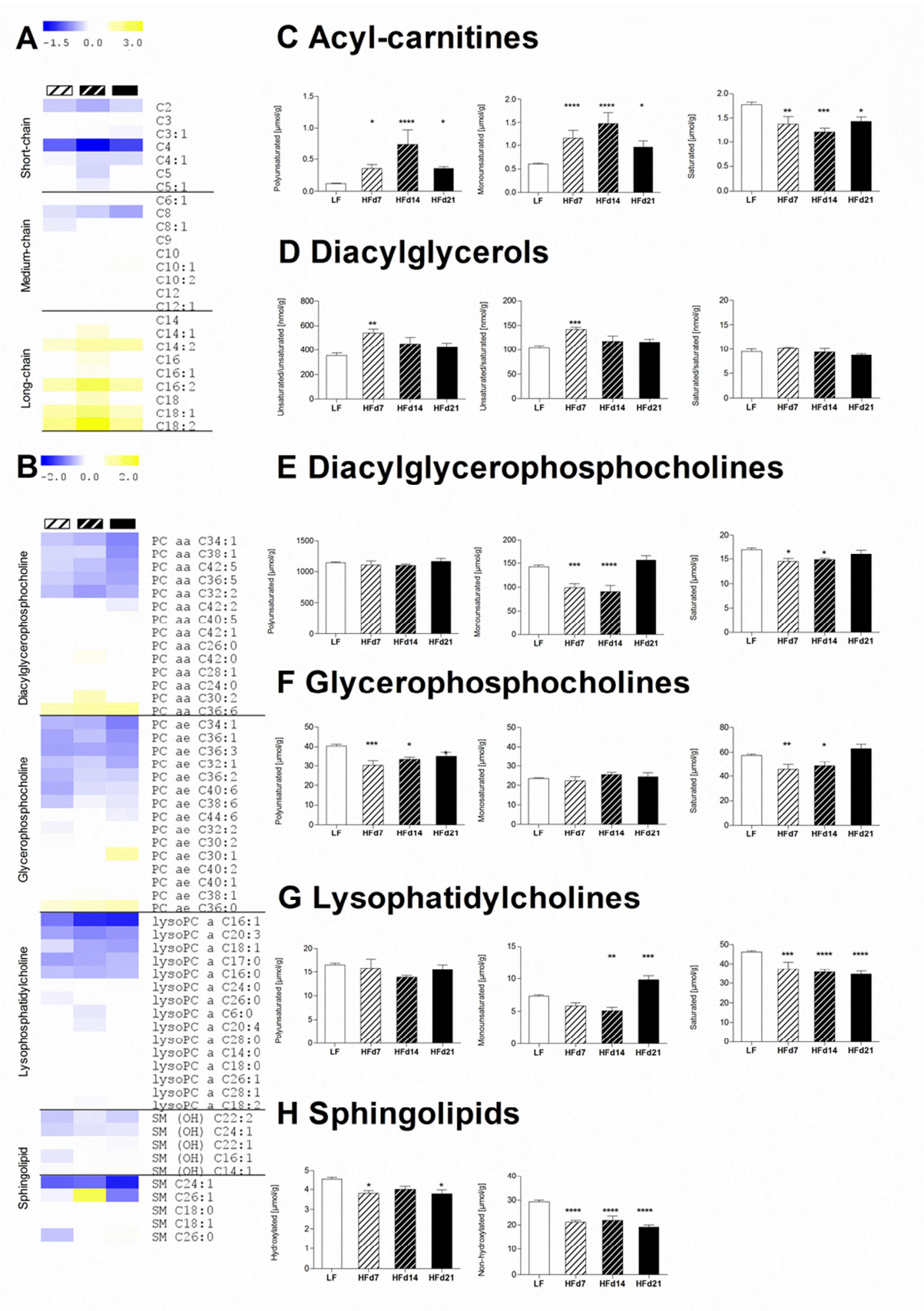
A
-1.5 0.0 3.0
Short-chain
Medium-chain
Long-chain
C2
C3
C3:1
C4
C4:1
C5
C5:1
C6:1
C8
C8:1
C9
C10
C10:1
C10:2
C12
C12:1
C14
C14:1
C14:2
C16
C16:1
C16:2
C18
C18:1
C18:2
C Acyl-carnitines
Polyunsaturated [µmol/g]
Monounsaturated [µmol/g]
Saturated [µmol/g]
D Diacylglycerols
Unsaturated/unsaturated [nmol/g]
Unsaturated/saturated [nmol/g]
Saturated/saturated [nmol/g]
B
-2.0 0.0 2.0
Diacylglycerophosphocholine
PC aa C34:1
PC aa C38:1
PC aa C42:5
PC aa C36:5
PC aa C32:2
PC aa C42:2
PC aa C40:5
PC aa C42:1
PC aa C26:0
PC aa C42:0
PC aa C28:1
PC aa C24:0
PC aa C30:2
PC aa C36:6
Glycerophosphocholine
PC ae C34:1
PC ae C36:1
PC ae C36:3
PC ae C32:1
PC ae C36:2
PC ae C40:6
PC ae C38:6
PC ae C44:6
PC ae C32:2
PC ae C30:2
PC ae C30:1
PC ae C40:2
PC ae C40:1
PC ae C38:1
PC ae C36:0
Lysophosphatidylcholine
lysoPC a C16:1
lysoPC a C20:3
lysoPC a C18:1
lysoPC a C17:0
lysoPC a C16:0
lysoPC a C24:0
lysoPC a C26:0
lysoPC a C6:0
lysoPC a C20:4
lysoPC a C28:0
lysoPC a C14:0
lysoPC a C18:0
lysoPC a C26:1
lysoPC a C28:1
lysoPC a C18:2
Sphingolipid
SM (OH) C22:2
SM (OH) C24:1
SM (OH) C22:1
SM (OH) C16:1
SM (OH) C14:1
SM C24:1
SM C26:1
SM C18:0
SM C18:1
SM C26:0
E Diacylglycerophosphocholines
F Glycerophosphocholines
G Lysophatidylcholines
H Sphingolipids
Hydroxylated [µmol/g]
Non-hydroxylated [µmol/g]
LF
HFd7
HFd14
HFd21

Membrane-associated proteins

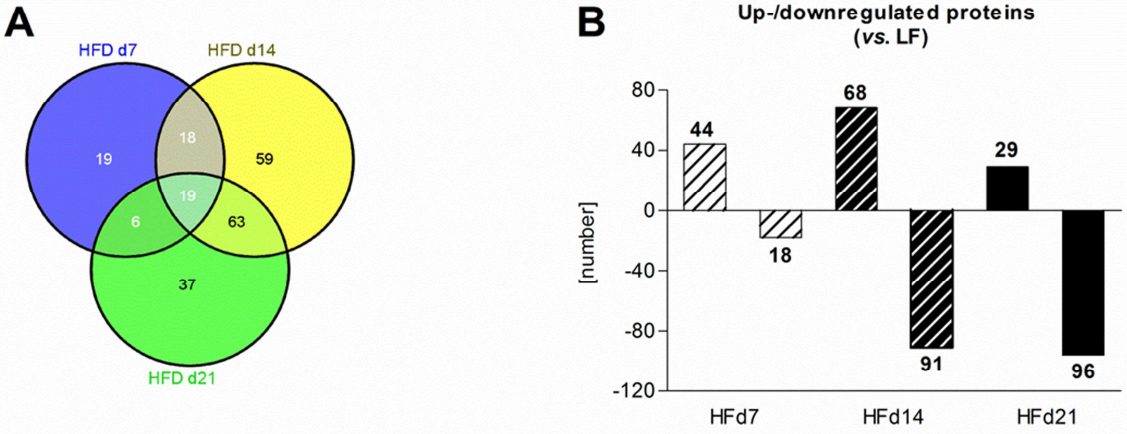

Networks based on mitochondria-associated proteins

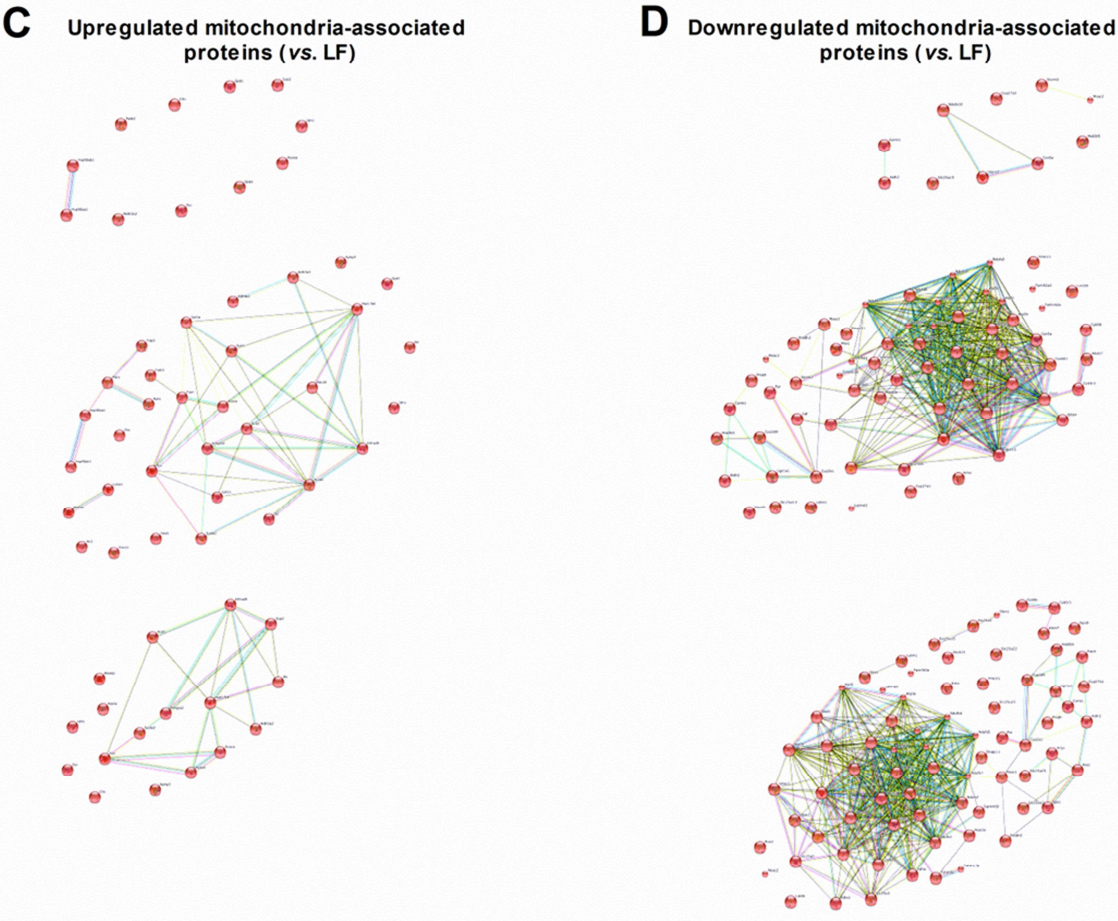

A Mitochondrial respiratory chain components

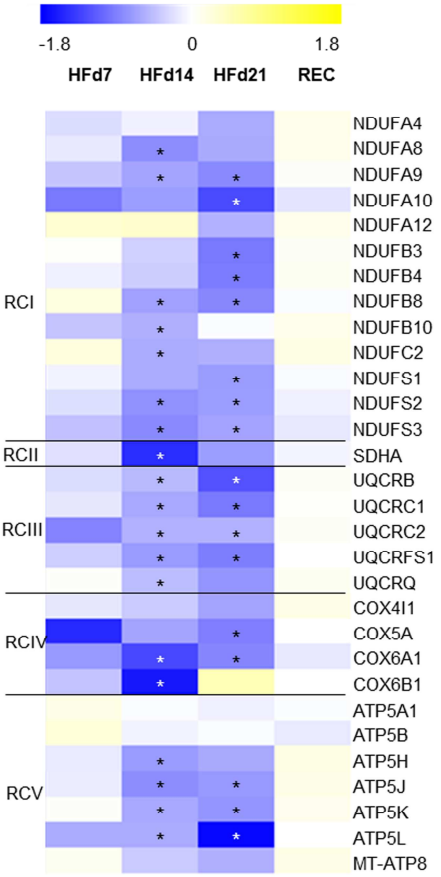

B Solute carriers of the inner mitochondrial membrane

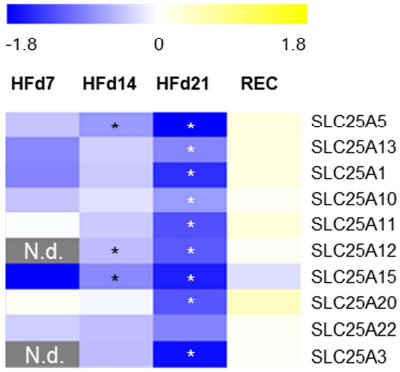

C Outer mitochondrial membrane channels

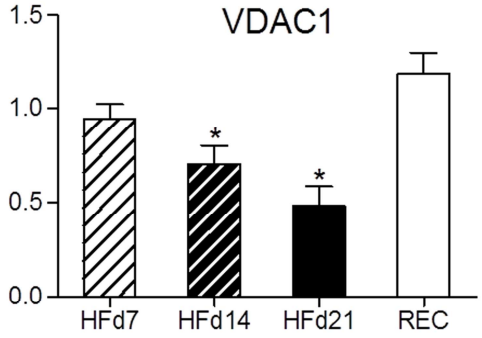

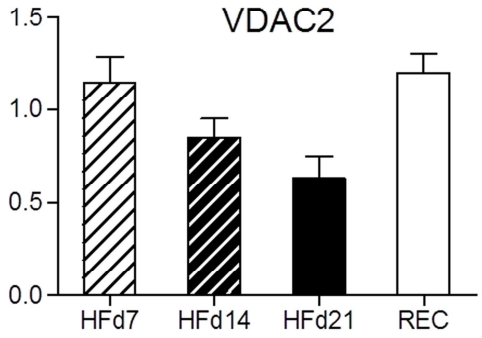

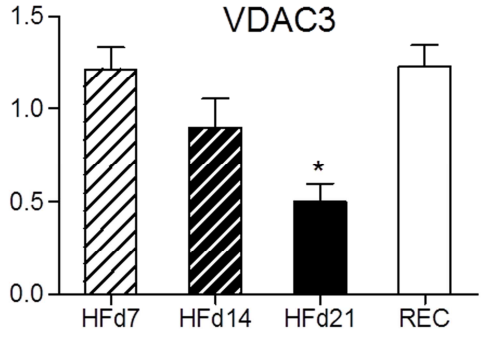

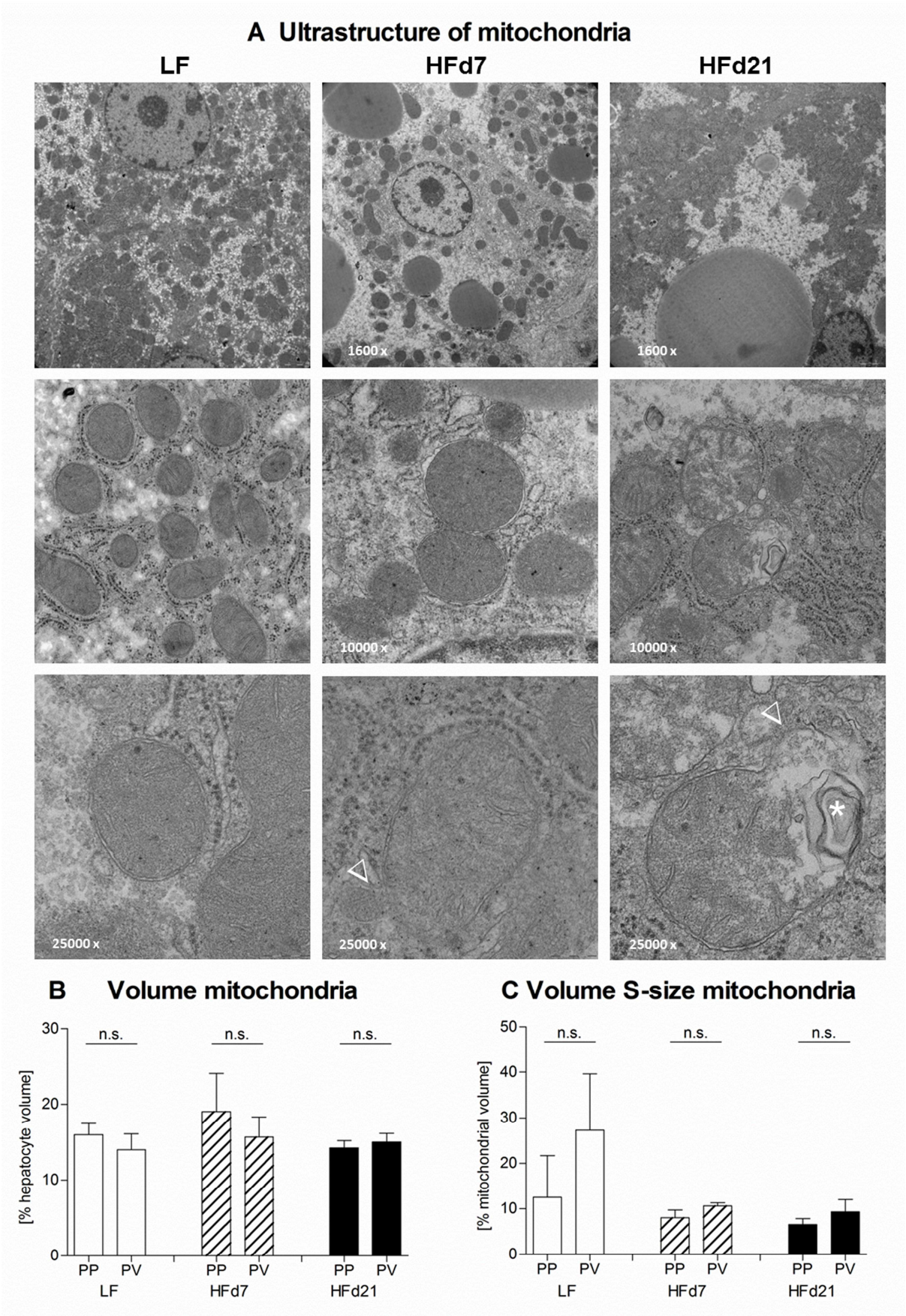
A Ultrastructure of mitochondria
LF
HFd7
HFd21
1600 x
1600 x
10000 x
10000 x
25000 x
25000 x
25000 x
B Volume mitochondria
[% hepatocyte volume]
30
20
10
0
n.s.
n.s.
n.s.
PP
PV
PP
PV
PP
PV
LF
HFd7
HFd21
C Volume S-size mitochondria
[% mitochondrial volume]
50
40
30
20
10
0
n.s.
n.s.
n.s.
PP
PV
PP
PV
PP
PV
LF
HFd7
HFd21

- pathophysiology of high-fat-diet mediated hepatic insulin resistance
- time-course study in mouse model
- comprehensive phenotypic, metabolomics, protemics and ultrastructural analyses
- temporal modifications in membrane lipid-signatures
- temporal decrease in mitochondrial membrane-associated proteins
- mitochondrial damage
- oxidative stress

Supplemental Table 1. Membrane-associated phospholipid signatures in livers during developing, HF-induced hepatic insulin resistance. *Via* t-metabolomics liver lipid profiles were assessed in male, random-fed mice following exposure to HF or LF (pooled) for 7, 14, or 21 days. The table depicts the concentrations of individual **A**) short-, medium- and long-chain carnitine acyl esters and **B**) phospholipids. Data are means±SEM. n=6-24/group. *p < 0.05; **p < 0.01; ***p < 0.001; ****p < 0.0001 *vs*. LF (ANOVA, Bonferroni). Abbreviations: PC aa diacylglycerophosphocholine (lecitine); PC ae, glycerophosphocholine (plasmalogen); lysoPC, lysophosphatidylcholine (lysolecithine); SM, sphingolipid.

A) Acyl-carnitines (µmol/l)	LF	HF d7	HF d14	HF d21
Carnitine	21.78 ± 0.58	18.07 ± 1.78*	17.30 ± 0.71**	21.37 ± 0.85
C2:0 (short-chain)	14.62 ± 0.38	11.21 ± 1.24**	10.16 ± 0.58****	11.68 ± 0.68**
C3:0 (short-chain)	0.86 ± 0.04	1.05 ± 0.18	0.87 ± 0.13	1.30 ± 0.19**
C3:1 (short-chain)	0.01 ± 0.00	0.01 ± 0.00	0.01 ± 0.00	0.01 ± 0.00
C4:0 (short-chain)	2.84 ± 0.22	1.52 ± 0.26*	1.03 ± 0.15***	1.37 ± 0.13**
C4:1 (short-chain)	0.03 ± 0.00	0.03 ± 0.00	0.02 ± 0.00**	0.02 ± 0.00**
C5:0 (short-chain)	0.55 ± 0.04	0.67 ± 0.11	0.44 ± 0.11	0.76 ± 0.09
C5:1(short-chain)	0.02 ± 0.00	0.02 ± 0.00	0.02 ± 0.00*	0.02 ± 0.00
C6:1 (medium-chain)	0.02 ± 0.00	0.02 ± 0.00	0.02 ± 0.00	0.02 ± 0.00
C8:0 (medium-chain)	0.16 ± 0.01	0.13 ± 0.02	0.12 ± 0.01	0.11 ± 0.01*
C8:1 (medium-chain)	0.01 ± 0.00	0.01 ± 0.00	0.01 ± 0.00	0.01 ± 0.00
C9:0 (medium-chain)	0.02 ± 0.00	0.02 ± 0.00	0.02 ± 0.00	0.02 ± 0.00*
C10:0 (medium-chain)	0.08 ± 0.00	0.08 ± 0.01	0.08 ± 0.00	0.09 ± 0.00
C10:1 (medium-chain)	0.07 ± 0.00	0.10 ± 0.01***	0.12 ± 0.01****	0.13 ± 0.01****
C10:2 (medium-chain)	0.02 ± 0.00	0.03 ± 0.00	0.03 ± 0.00***	0.03 ± 0.00****
C12:0 (medium-chain)	0.05 ± 0.00	0.05 ± 0.00	0.05 ± 0.01	0.05 ± 0.00
C12:1 (medium-chain)	0.09 ± 0.00	0.10 ± 0.01	0.09 ± 0.01	0.10 ± 0.01

C14:0 (long-chain)	0.07 ± 0.00	0.08 ± 0.01	0.09 ± 0.02	0.07 ± 0.00
C14:1 (long-chain)	0.03 ± 0.00	0.04 ± 0.00	0.06 ± 0.01****	0.04 ± 0.00
C14:2 (long-chain)	0.01 ± 0.00	0.01 ± 0.00*	0.02 ± 0.01****	0.02 ± 0.00***
C16:0 (long-chain)	0.16 ± 0.01	0.21 ± 0.03	0.31 ± 0.07****	0.17 ± 0.02
C16:1 (long-chain)	0.08 ± 0.00	0.12 ± 0.01	0.15 ± 0.03****	0.09 ± 0.01
C16:2 (long-chain)	0.01 ± 0.00	0.03 ± 0.00	0.05 ± 0.02****	0.03 ± 0.00*
C18:0 (long-chain)	0.07 ± 0.00	0.11 ± 0.02	0.15 ± 0.03****	0.10 ± 0.02
C18:1 (long-chain)	0.26 ± 0.02	0.75 ± 0.14****	1.00 ± 0.21****	0.55 ± 0.12*
C18:2 (long-chain)	0.08 ± 0.01	0.29 ± 0.05*	0.63 ± 0.22****	0.28 ± 0.03

B) Diacylglycerophosphocholines (µmol/l)	LF	HF d7	HF d14	HF d21
PC aa C24:0	0.20 ± 0.01	0.23 ± 0.02	0.26 ± 0.04	0.23 ± 0.02
PC aa C26:0	0.70 ± 0.01	0.67 ± 0.02	0.76 ± 0.07	0.68 ± 0.03
PC aa C28:1	0.16 ± 0.01	0.17 ± 0.01	0.20 ± 0.02	0.18 ± 0.01
PC aa C30:0	0.69 ± 0.02	0.51 ± 0.03	0.51 ± 0.01	0.46 ± 0.01
PC aa C30:2	0.06 ± 0.00	0.07 ± 0.01	0.09 ± 0.02	0.06 ± 0.01
PC aa C32:0	13.17 ± 0.32	11.32 ± 0.42	11.12 ± 0.37	10.48 ± 0.50
PC aa C32:1	12.03 ± 0.74	3.90 ± 0.98	2.75 ± 0.41	2.41 ± 0.17
PC aa C32:2	2.59 ± 0.08	1.74 ± 0.17	1.48 ± 0.11	1.66 ± 0.08
PC aa C32:3	0.15 ± 0.00	0.16 ± 0.01	0.16 ± 0.01	0.16 ± 0.01
PC aa C34:1	110.47 ± 2.63	76.53 ± 6.01	70.27 ± 11.09	56.44 ± 2.76
PC aa C34:2	163.42 ± 1.80	156.43 ± 7.15	155.71 ± 2.04	151.86 ± 2.50
PC aa C34:3	28.66 ± 0.66	19.35 ± 1.88	17.27 ± 0.88	16.63 ± 0.50
PC aa C34:4	2.37 ± 0.06	2.94 ± 0.35	2.95 ± 0.29	3.08 ± 0.31
PC aa C36:0	0.85 ± 0.02	0.67 ± 0.03	0.73 ± 0.09	0.62 ± 0.06
PC aa C36:1	18.59 ± 0.72	18.03 ± 1.59	16.96 ± 1.60	13.97 ± 0.70
PC aa C36:2	115.92 ± 2.03	125.00 ± 7.42	124.00 ± 2.37	120.14 ± 4.07
PC aa C36:3	116.97 ± 1.95	105.63 ± 7.75	104.44 ± 4.20	100.96 ± 1.82

PC aa C36:4	163.97	±	1.66	163.29	±	4.78	157.29	±	1.44	156.29	±	1.94
PC aa C36:5	20.38	±	0.52	14.60	±	1.46	13.24	±	0.78	12.11	±	0.36
PC aa C36:6	1.12	±	0.03	1.91	±	0.28	2.38	±	0.33	2.49	±	0.32
PC aa C38:0	1.44	±	0.03	1.04	±	0.09	1.18	±	0.07	1.11	±	0.05
PC aa C38:1	0.38	±	0.02	0.29	±	0.03	0.29	±	0.04	0.21	±	0.05
PC aa C38:3	39.40	±	1.25	42.37	±	4.96	41.57	±	2.40	39.46	±	1.65
PC aa C38:4	138.68	±	2.03	147.43	±	6.29	144.86	±	1.71	143.14	±	2.19
PC aa C38:5	115.66	±	1.92	118.70	±	7.62	113.83	±	5.59	110.29	±	2.58
PC aa C38:6	151.84	±	2.21	138.54	±	9.30	145.29	±	2.63	145.14	±	2.63
PC aa C40:1	0.37	±	0.01	0.35	±	0.01	0.37	±	0.02	0.33	±	0.01
PC aa C40:2	0.55	±	0.02	0.53	±	0.04	0.57	±	0.05	0.47	±	0.02
PC aa C40:3	1.11	±	0.03	0.82	±	0.06	0.80	±	0.04	0.70	±	0.02
PC aa C40:4	5.79	±	0.16	4.88	±	0.40	4.91	±	0.26	4.25	±	0.24
PC aa C40:5	18.34	±	0.52	21.04	±	1.71	18.63	±	1.60	16.46	±	0.53
PC aa C40:6	49.90	±	1.16	42.03	±	4.00	46.46	±	1.37	46.43	±	2.12
PC aa C42:0	0.18	±	0.01	0.23	±	0.04	0.27	±	0.05	0.19	±	0.02
PC aa C42:1	0.13	±	0.01	0.15	±	0.02	0.17	±	0.03	0.12	±	0.01
PC aa C42:2	0.23	±	0.01	0.21	±	0.02	0.26	±	0.04	0.19	±	0.01
PC aa C42:4	0.35	±	0.01	0.31	±	0.02	0.34	±	0.02	0.29	±	0.02
PC aa C42:5	0.80	±	0.02	0.59	±	0.05	0.54	±	0.03	0.46	±	0.01
PC aa C42:6	1.75	±	0.04	1.26	±	0.10	1.26	±	0.05	1.14	±	0.04

Glycerophosphocholines (plasmalogen, µmol/l)	LF			HF d7			HF d14			HF d21		
PC ae C30:0	0.13	±	0.00	0.12	±	0.00	0.11	±	0.01	0.11	±	0.00
PC ae C30:1	0.09	±	0.00	0.09	±	0.01	0.13	±	0.03	0.09	±	0.01
PC ae C30:2	0.10	±	0.00	0.08	±	0.00	0.10	±	0.01	0.09	±	0.01
PC ae C32:1	0.40	±	0.01	0.27	±	0.02	0.29	±	0.03	0.24	±	0.01

PC ae C32:2	0.14	± 0.00	0.12	± 0.00	0.14	± 0.02	0.13	± 0.01
PC ae C34:0	0.34	± 0.01	0.27	± 0.01	0.28	± 0.01	0.27	± 0.01
PC ae C34:1	3.39	± 0.10	2.18	± 0.17	2.13	± 0.31	1.68	± 0.11
PC ae C34:2	2.36	± 0.09	1.41	± 0.14	1.64	± 0.11	1.56	± 0.11
PC ae C34:3	0.26	± 0.01	0.21	± 0.01	0.25	± 0.02	0.21	± 0.01
PC ae C36:0	0.33	± 0.01	0.51	± 0.06	0.53	± 0.04	0.55	± 0.04
PC ae C36:1	2.61	± 0.06	1.54	± 0.14	1.77	± 0.14	1.44	± 0.05
PC ae C36:2	6.11	± 0.16	3.93	± 0.35	4.54	± 0.23	4.41	± 0.24
PC ae C36:3	2.29	± 0.06	1.34	± 0.15	1.38	± 0.06	1.33	± 0.05
PC ae C36:4	3.75	± 0.11	2.77	± 0.27	3.01	± 0.12	2.90	± 0.11
PC ae C36:5	0.96	± 0.02	0.83	± 0.08	0.83	± 0.01	0.80	± 0.04
PC ae C38:0	7.58	± 0.20	5.72	± 0.58	5.87	± 0.21	5.88	± 0.20
PC ae C38:1	0.71	± 0.02	0.76	± 0.07	1.01	± 0.13	1.00	± 0.08
PC ae C38:2	2.70	± 0.06	1.83	± 0.14	1.98	± 0.12	1.95	± 0.12
PC ae C38:3	2.47	± 0.05	1.59	± 0.16	1.77	± 0.11	1.65	± 0.07
PC ae C38:4	9.81	± 0.33	7.65	± 0.72	8.77	± 0.42	8.75	± 0.50
PC ae C38:5	4.29	± 0.09	3.88	± 0.35	3.96	± 0.40	3.60	± 0.21
PC ae C38:6	1.79	± 0.06	1.24	± 0.12	1.53	± 0.11	1.44	± 0.06
PC ae C40:0	46.75	± 0.99	37.20	± 3.48	40.23	± 3.39	40.71	± 2.06
PC ae C40:1	14.38	± 0.35	15.83	± 1.74	18.33	± 1.00	18.91	± 0.79
PC ae C40:2	0.78	± 0.02	0.81	± 0.08	1.02	± 0.08	0.96	± 0.05
PC ae C40:3	0.92	± 0.02	0.82	± 0.07	0.92	± 0.08	0.85	± 0.04
PC ae C40:4	3.72	± 0.10	2.77	± 0.23	2.87	± 0.11	2.77	± 0.14
PC ae C40:5	2.07	± 0.04	1.65	± 0.13	1.73	± 0.06	1.65	± 0.07
PC ae C40:6	3.39	± 0.12	2.07	± 0.23	2.60	± 0.23	2.65	± 0.17
PC ae C42:0	2.27	± 0.06	1.71	± 0.17	1.64	± 0.09	1.55	± 0.05
PC ae C42:1	1.72	± 0.04	1.68	± 0.16	1.95	± 0.17	1.95	± 0.10
PC ae C42:2	1.31	± 0.04	1.38	± 0.11	1.40	± 0.12	1.33	± 0.06

PC ae C42:3	2.95 ± 0.08	2.20 ± 0.20	2.48 ± 0.11	2.72 ± 0.12
PC ae C42:4	0.32 ± 0.01	0.26 ± 0.02	0.30 ± 0.02	0.26 ± 0.01
PC ae C42:5	0.75 ± 0.01	0.63 ± 0.03	0.65 ± 0.02	0.61 ± 0.01
PC ae C44:3	0.16 ± 0.00	0.13 ± 0.01	0.15 ± 0.02	0.13 ± 0.00
PC ae C44:4	0.17 ± 0.01	0.13 ± 0.01	0.15 ± 0.01	0.12 ± 0.01
PC ae C44:5	0.22 ± 0.01	0.15 ± 0.01	0.18 ± 0.02	0.16 ± 0.01
PC ae C44:6	0.15 ± 0.00	0.14 ± 0.01	0.15 ± 0.01	0.13 ± 0.01

Lysophosphatidylcholines (µmol/l)	LFD	HFD d7	HFD d14	HFD d21
lysoPC a C14:0	3.31 ± 0.01	3.24 ± 0.02	3.28 ± 0.02	3.33 ± 0.03
lysoPC a C16:0	27.52 ± 0.50	18.62 ± 2.27	17.67 ± 1.07	18.34 ± 0.83
lysoPC a C16:1	0.42 ± 0.02	0.20 ± 0.03	0.14 ± 0.01	0.14 ± 0.01
lysoPC a C17:0	0.45 ± 0.01	0.26 ± 0.03	0.27 ± 0.02	0.29 ± 0.02
lysoPC a C18:0	13.98 ± 0.26	14.36 ± 1.57	13.80 ± 0.48	14.33 ± 0.55
lysoPC a C18:1	5.15 ± 0.22	3.92 ± 0.46	3.11 ± 0.57	3.00 ± 0.34
lysoPC a C18:2	9.01 ± 0.21	8.66 ± 1.04	7.90 ± 0.38	9.44 ± 0.45
lysoPC a C20:3	0.96 ± 0.04	0.56 ± 0.07	0.49 ± 0.02	0.53 ± 0.02
lysoPC a C20:4	6.58 ± 0.19	6.63 ± 0.83	5.46 ± 0.31	6.06 ± 0.28
lysoPC a C24:0	0.27 ± 0.01	0.24 ± 0.02	0.28 ± 0.03	0.24 ± 0.02
lysoPC a C26:0	0.33 ± 0.01	0.28 ± 0.01	0.32 ± 0.04	0.30 ± 0.02
lysoPC a C26:1	1.51 ± 0.01	1.48 ± 0.02	1.57 ± 0.06	1.55 ± 0.03
lysoPC a C28:0	0.22 ± 0.01	0.21 ± 0.01	0.24 ± 0.02	0.21 ± 0.01
lysoPC a C28:1	0.23 ± 0.01	0.24 ± 0.02	0.30 ± 0.05	0.24 ± 0.03

Phosphocholines, hydroxylated (ceramide; µmol/l)	LFD	HFD d7	HFD d14	HFD d21
SM (OH) C14:1	0.50 ± 0.02	0.44 ± 0.04	0.52 ± 0.02	0.52 ± 0.03
SM (OH) C16:1	0.14 ± 0.00	0.11 ± 0.01	0.13 ± 0.01	0.12 ± 0.01

SM (OH) C22:1	2.09 ±	0.04	2.00 ±	0.05	1.92 ±	0.07	1.82 ±	0.11
SM (OH) C22:2	1.63 ±	0.06	1.14 ±	0.07	1.31 ±	0.12	1.18 ±	0.07
SM (OH) C24:1	0.16 ±	0.00	0.11 ±	0.01	0.12 ±	0.01	0.13 ±	0.01
Phosphocholines (ceramide; µmol/l)								
SM C16:0	9.22 ±	0.27	7.73 ±	0.55	8.32 ±	0.31	7.88 ±	0.33
SM C16:1	0.75 ±	0.01	0.62 ±	0.06	0.67 ±	0.02	0.67 ±	0.04
SM C18:0	0.95 ±	0.03	0.94 ±	0.06	1.11 ±	0.07	0.97 ±	0.06
SM C18:1	0.14 ±	0.00	0.14 ±	0.01	0.17 ±	0.01	0.16 ±	0.01
SM C24:0	7.14 ±	0.12	6.66 ±	0.23	6.30 ±	0.15	5.84 ±	0.27
SM C24:1	11.15 ±	0.39	4.78 ±	0.82	5.11 ±	1.54	3.54 ±	0.39
SM C26:0	0.01 ±	0.00	0.01 ±	0.00	0.01 ±	0.00	0.02 ±	0.00

Supplemental Table 2. Membrane-associated diacylglycerol signatures in livers during developing HF-induced hepatic insulin resistance. Liver membrane-associated diacylglycerol species were determined in 6 hour fasting male mice following exposure to HF or LF (pooled) for 7, 14, or 21 days. Data are means±SEM. n=6-9/group. *p < 0.05; **p < 0.01; ***p < 0.001; ****p < 0.0001 *vs*. LF (ANOVA, Bonferroni).

Diacylglycerol (nmol/g)	LF		HF d7		HF d14		HF d21	
C16:0/C16:0	3.76 ±	0.24	3.41 ±	0.13	3.64 ±	0.69	3.08 ±	0.19
C18:0/C16:0	1.57 ±	0.12	1.31 ±	0.04	1.51 ±	0.24	1.29 ±	0.10
C18:0/C18:0	4.14 ±	0.26	5.35 ±	0.21	5.89 ±	0.88	4.41 ±	0.18
C18:1/C18:1	112.19 ±	9.55	71.39 ±	4.06	76.43 ±	13.61	57.06 ±	2.22
C18:1/C18:2	62.66 ±	4.85	82.02 ±	4.44	98.29 ±	19.66	73.44 ±	3.19
C18:2/C18:2	27.57 ±	2.93	71.41 ±	5.00	98.49 ±	25.65	82.22 ±	8.76

C20:4/C20:5	150.46	±	13.14	314.90	±	30.56	298.22	±	73.57	209.67	±	32.31
C16:0/C20:4	5.03	±	0.35	6.57	±	0.34	6.46	±	1.27	4.75	±	0.32
C18:1/C16:0	26.78	±	1.66	20.40	±	1.05	19.39	±	3.83	15.68	±	1.56
C16:0/C18:2	59.40	±	3.87	96.55	±	3.81	102.38	±	22.29	80.27	±	4.14
C18:2/C18:0	4.24	±	0.28	7.26	±	0.29	8.55	±	1.98	7.16	±	0.42
C18:1/C18:0	2.88	±	0.17	2.40	±	0.10	2.59	±	0.52	2.15	±	0.13
C18:0/C20:4	4.29	±	0.35	8.78	±	0.83	8.53	±	2.06	5.98	±	0.78

IPI	Gene symb	Species	Gene Name
IPI00127815	SRPX	Mus muscu	sushi-repeat-containing protein; retinitis pigmentosa GTPase regulator
IPI00608021	Ddi2	Mus muscu	regulatory solute carrier protein, family 1, member 1; DNA-damage inducible protein 2
IPI00624211	RASAL3	Mus muscu	RIKEN cDNA A430107D22 gene
IPI00137736	Gm3511	Mus muscu	similar to 40S ribosomal protein S28; predicted gene 10443; predicted gene 12943; predicted gene 13192; simila
IPI00222142	Serpina7	Mus muscu	serine (or cysteine) peptidase inhibitor, clade A (alpha-1 antiproteinase, antitrypsin), member 7
IPI00137731	stam	Mus muscu	signal transducing adaptor molecule (SH3 domain and ITAM motif) 1
IPI00137730	PEBP1	Mus muscu	phosphatidylethanolamine binding protein 1
IPI00624210	Gm4952	Mus muscu	predicted gene 4952
IPI00262094	BICD1	Mus muscu	bicaudal D homolog 1 (Drosophila)
IPI00464312	DENND3	Mus muscu	DENN/MADD domain containing 3
IPI00109437	PIR	Mus muscu	pirin
IPI00130828	TULP3	Mus muscu	tubby-like protein 3
IPI00222135	TRPM3	Mus muscu	transient receptor potential cation channel, subfamily M, member 3
IPI00331728	BMPER	Mus muscu	BMP-binding endothelial regulator
IPI00464318	Pcf11	Mus muscu	cleavage and polyadenylation factor subunit homolog (S. cerevisiae)
IPI00402998	KLHDC10	Mus muscu	kelch domain containing 10
IPI00109434	D10Ertd61	Mus muscu	DNA segment, Chr 10, ERATO Doi 610, expressed
IPI00111877	SSBP1	Mus muscu	predicted gene 12115; single-stranded DNA binding protein 1
IPI00137725	Aup1	Mus muscu	ancient ubiquitous protein 1
IPI00111876	ABHD14B	Mus muscu	abhydrolase domain containing 14b
IPI00137724	wbp2nl	Mus muscu	WBP2 N-terminal like
IPI00222125	COMTD1	Mus muscu	catechol-O-methyltransferase domain containing 1
IPI00464304	CEP152	Mus muscu	centrosomal protein 152
IPI00153903	CLYBL	Mus muscu	citrate lyase beta like
IPI00331738	LOC10004	Mus muscu	tripartite motif-containing 21; similar to Tripartite motif protein 21
IPI00331734	H2AFZ	Mus muscu	H2A histone family, member Z; predicted gene 6722; predicted gene 8203
IPI00111842	NARF	Mus muscu	nuclear prelamin A recognition factor
IPI00608004	Ccdc88b	Mus muscu	coiled-coil domain containing 88B
IPI00122772	THAP7	Mus muscu	THAP domain containing 7
IPI00649885	ACADVL	Mus muscu	acyl-Coenzyme A dehydrogenase, very long chain
IPI00409462	Bat1a	Mus muscu	HLA-B-associated transcript 1A
IPI00109420	Kif5a	Mus muscu	kinesin family member 5A
IPI00608001	CHD5	Mus muscu	chromodomain helicase DNA binding protein 5
IPI00313390	CHCHD6	Mus muscu	coiled-coil-helix-coiled-coil-helix domain containing 6
IPI00153939	LOC10004	Mus muscu	OTU domain containing 7A; hypothetical protein LOC100044257
IPI00137713	4930522N	Mus muscu	RIKEN cDNA 4930522N08 gene
IPI00225192	NUP54	Mus muscu	nucleoporin 54
IPI00130804	ech1	Mus muscu	enoyl coenzyme A hydratase 1, peroxisomal
IPI00230204	GOT1	Mus muscu	similar to Aspartate aminotransferase, cytoplasmic (Transaminase A) (Glutamate oxaloacetate transaminase 1);
IPI00230205	PDPN	Mus muscu	podoplanin
IPI00110719	PIPOX	Mus muscu	pipecolic acid oxidase
IPI00109419	Kif4	Mus muscu	kinesin family member 4
IPI00177214	Igh-6	Mus muscu	immunoglobulin heavy chain 6 (heavy chain of IgM)
IPI00406098	Gm9997	Mus muscu	predicted gene 9997
IPI00331707	LOC10004	Mus muscu	similar to Hmgcs1 protein; 3-hydroxy-3-methylglutaryl-Coenzyme A synthase 1
IPI00269896	LOC10004	Mus muscu	IKAROS family zinc finger 4; similar to helios
IPI00462075	Gm4335	Mus muscu	predicted gene 4691; predicted gene 6944; predicted gene 10290; predicted gene 10566; predicted gene 10291;
IPI00665466	FRMD6	Mus muscu	predicted gene 5780; FERM domain containing 6
IPI00649890	0610037L1	Mus muscu	RIKEN cDNA 0610037L13 gene
IPI00462072	Gm5506	Mus muscu	predicted gene 4735; enolase 1, alpha non-neuron; similar to enolase 1, alpha non-neuron; hypothetical protein
IPI00224866	Fbxw19	Mus muscu	F-box and WD-40 domain protein 19
IPI00880407	UFM1	Mus muscu	ubiquitin-fold modifier 1
IPI00110721	GLOD4	Mus muscu	glyoxalase domain containing 4
IPI00111855	Hsd3b3	Mus muscu	hydroxy-delta-5-steroid dehydrogenase, 3 beta- and steroid delta-isomerase 3
IPI00110724	LOC10004	Mus muscu	predicted gene 2157; similar to ribosomal protein L22 like 1; ribosomal protein L22 like 1
IPI00111854	HRK	Mus muscu	harakiri, BCL2 interacting protein (contains only BH3 domain)
IPI00129928	Fh1	Mus muscu	fumarate hydratase 1
IPI00110729	Chmp5	Mus muscu	chromatin modifying protein 5
IPI00331710	ACAD9	Mus muscu	acyl-Coenzyme A dehydrogenase family, member 9
IPI00222147	rufy1	Mus muscu	RUN and FYVE domain containing 1
IPI00331711	BRCA1	Mus muscu	breast cancer 1
IPI00230212	Gm5562	Mus muscu	similar to Glutathione S-transferase Mu 1 (GST class-mu 1) (Glutathione S-transferase GT8.7) (pmGT10) (GST 1-1)
IPI00224870	Col9a3	Mus muscu	collagen, type IX, alpha 3
IPI00321407	cul4a	Mus muscu	cullin 4A
IPI00453906	Efha1	Mus muscu	EF hand domain family A1
IPI00336913	TRIM29	Mus muscu	tripartite motif-containing 29
IPI00153959	STAB1	Mus muscu	stabilin 1
IPI00222180	LOC10004	Mus muscu	valyl-tRNA synthetase 2, mitochondrial (putative); similar to valyl-tRNA synthetase 2-like
IPI00109482	DDAH1	Mus muscu	dimethylarginine dimethylaminohydrolase 1
IPI00123806	Trim41	Mus muscu	tripartite motif-containing 41
IPI00122757	LOC10004	Mus muscu	Kruppel-like factor 3 (basic); similar to BKLF
IPI00665485	LOC67671	Mus muscu	similar to Cys2/His2 zinc finger protein (rKr1); zinc finger protein 180
IPI00322562	Gm6204	Mus muscu	predicted gene 6204; ribosomal protein S14
IPI00127841	LOC63122	Mus muscu	solute carrier family 25 (mitochondrial carrier, adenine nucleotide translocator), member 5; similar to ADP/ATP t
IPI00336923	Zfp445	Mus muscu	zinc finger protein 445
IPI00110705	Prdxdd1	Mus muscu	non-protein coding RNA 117
IPI00225114	D730040F1	Mus muscu	RIKEN cDNA D730040F13 gene
IPI00336929	2310014H	Mus muscu	RIKEN cDNA 2310014H01 gene
IPI00129985	CDR2	Mus muscu	cerebellar degeneration-related 2
IPI00665496	Gm101	Mus muscu	predicted gene 101
IPI00230232	Cacna1d	Mus muscu	calcium channel, voltage-dependent, L type, alpha 1D subunit
IPI00225123	GBA2	Mus muscu	glucosidase beta 2
IPI00110708	Ccdc51	Mus muscu	coiled-coil domain containing 51
IPI00406045	PIK3R4	Mus muscu	phosphatidylinositol 3 kinase, regulatory subunit, polypeptide 4, p150
IPI00153942	IFT81	Mus muscu	intraflagellar transport 81 homolog (Chlamydomonas)
IPI00110709	Wbscr22	Mus muscu	Williams Beuren syndrome chromosome region 22
IPI00321421	PLEKHG3	Mus muscu	pleckstrin homology domain containing, family G (with RhoGef domain) member 3
IPI00322551	PLCD4	Mus muscu	phospholipase C, delta 4
IPI00130840	cope	Mus muscu	coatomer protein complex, subunit epsilon
IPI00284769	STARD5	Mus muscu	StAR-related lipid transfer (START) domain containing 5
IPI00651800	Zmiz1	Mus muscu	RIKEN cDNA D930049A15 gene; zinc finger, MIZ-type containing 1
IPI00111884	SLC25A35	Mus muscu	solute carrier family 25, member 35
IPI00111885	Uqcrc1	Mus muscu	ubiquinol-cytochrome c reductase core protein 1
IPI00177257	rnf112	Mus muscu	ring finger protein 112
IPI00230248	TLE1	Mus muscu	transducin-like enhancer of split 1, homolog of Drosophila E(spl)
IPI00322589	e2f6	Mus muscu	E2F transcription factor 6
IPI00464335	psd	Mus muscu	pleckstrin and Sec7 domain containing
IPI00310035	FAH	Mus muscu	fumarylacetoacetate hydrolase
IPI00153976	ARMC7	Mus muscu	armadillo repeat containing 7
IPI00138892	Gm5928	Mus muscu	predicted gene 5928; predicted gene 12617; predicted gene 4802; similar to ribosomal protein S27a; predicted g
IPI00224825	D130020L	Mus muscu	RIKEN cDNA D130020L05 gene
IPI00322581	FCRLA	Mus muscu	Fc receptor-like A
IPI00122740	macrod1	Mus muscu	MACRO domain containing 1
IPI00109455	Nudt16	Mus muscu	nudix (nucleoside diphosphate linked moiety X)-type motif 16
IPI00130833	FKBP8	Mus muscu	FK506 binding protein 8
IPI00122743	Dars	Mus muscu	aspartyl-tRNA synthetase
IPI00357734	ZDBF2	Mus muscu	zinc finger, DBF-type containing 2
IPI00853967	ptrh2	Mus muscu	peptidyl-tRNA hydrolase 2
IPI00129964	Gm14270	Mus muscu	HCLS1 associated X-1; silica-induced gene 111
IPI00129963	phyH	Mus muscu	phytanoyl-CoA hydroxylase
IPI00270806	4930590J0	Mus muscu	RIKEN cDNA 4930590J08 gene
IPI00321446	Prkca	Mus muscu	protein kinase C, alpha
IPI00222188	COL1A2	Mus muscu	collagen, type I, alpha 2
IPI00322575	Abca8a	Mus muscu	ATP-binding cassette, sub-family A (ABC1), member 8a
IPI00177249	TMEM168	Mus muscu	transmembrane protein 168
IPI00407122	LOC10004	Mus muscu	similar to TAF4A RNA polymerase II, TATA box binding protein (TBP)-associated factor; predicted gene 5785
IPI00453958	DZIP1	Mus muscu	DAZ interacting protein 1
IPI00459639	FRMD8	Mus muscu	FERM domain containing 8
IPI00462013	SETBP1	Mus muscu	SET binding protein 1
IPI00409405	CFL1	Mus muscu	cofilin 1, non-muscle; similar to Cofilin-1 (Cofilin, non-muscle isoform); predicted gene 6180
IPI00664424	NEB	Mus muscu	nebulin
IPI00336958	ZC3H15	Mus muscu	predicted gene 5909; zinc finger CCCH-type containing 15
IPI00226218	Mettl7a1	Mus muscu	methyltransferase like 7A1
IPI00281355	LOC10004	Mus muscu	grainyhead-like 1 (Drosophila); similar to Grhl1 protein
IPI00131954	D17Wsu10	Mus muscu	DNA segment, Chr 17, Wayne State University 104, expressed
IPI00756198	KNTC1	Mus muscu	kinetochore associated 1
IPI00453962	OSBP2	Mus muscu	oxysterol binding protein 2; similar to oxysterol binding protein 2
IPI00138860	golga4	Mus muscu	golgi autoantigen, golgin subfamily a, 4
IPI00131949	Asb11	Mus muscu	ankyrin repeat and SOCS box-containing 11
IPI00322513	igfbp7	Mus muscu	insulin-like growth factor binding protein 7
IPI00407130	Gm6560	Mus muscu	predicted gene 6560; predicted gene 2124; predicted gene 6992; pyruvate kinase, muscle; similar to M2-type py
IPI00226212	KLHL31	Mus muscu	kelch-like 31 (Drosophila)
IPI00459652	Rnf8	Mus muscu	RIKEN cDNA 1300018I05 gene; ring finger protein 8
IPI00226205	Tapbp	Mus muscu	TAP binding protein
IPI00409412	Cyp2c67	Mus muscu	cytochrome P450, family 2, subfamily c, polypeptide 40; similar to RIKEN cDNA C730004C24 gene; cytochrome P
IPI00223751	ARHGAP12	Mus muscu	Rho GTPase activating protein 12
IPI00608098	Srcap	Mus muscu	Snf2-related CREBBP activator protein
IPI00608097	npepps	Mus muscu	aminopeptidase puromycin sensitive
IPI00652902	gnai2	Mus muscu	guanine nucleotide binding protein (G protein), alpha inhibiting 2; similar to Guanine nucleotide-binding protein
IPI00661414	arpc2	Mus muscu	predicted gene 5492; actin related protein 2/3 complex, subunit 2
IPI00464391	STAU1	Mus muscu	staufen (RNA binding protein) homolog 1 (Drosophila)
IPI00223757	Akr1b3	Mus muscu	aldo-keto reductase family 1, member B3 (aldose reductase)
IPI00321499	BCL2L13	Mus muscu	BCL2-like 13 (apoptosis facilitator)
IPI00322542	LOC67764	Mus muscu	histocompatibility 2, T region locus 23; similar to RT1 class Ib, locus H2-Q-like, grc region
IPI00453973	klhl5	Mus muscu	kelch-like 5 (Drosophila)
IPI00314439	psmd3	Mus muscu	proteasome (prosome, macropain) 26S subunit, non-ATPase, 3
IPI00311940	SEC1	Mus muscu	secretory blood group 1
IPI00132002	Mgst3	Mus muscu	microsomal glutathione S-transferase 3
IPI00108895	psmc4	Mus muscu	proteasome (prosome, macropain) 26S subunit, ATPase, 4
IPI00317309	ANXA5	Mus muscu	annexin A5
IPI00453981	fdxr	Mus muscu	ferredoxin reductase
IPI00453983	KLHL4	Mus muscu	kelch-like 4 (Drosophila)
IPI00226234	plaa	Mus muscu	phospholipase A2, activating protein
IPI00122702	Tas2r103	Mus muscu	predicted gene, EG667992; similar to Taste receptor type 2 member 10 (T2R10) (Taste receptor family B membe
IPI00226228	Azi1	Mus muscu	5-azacytidine induced gene 1
IPI00123838	Bach2	Mus muscu	BTB and CNC homology 2
IPI00137787	rpl8	Mus muscu	ribosomal protein L8; similar to 60S ribosomal protein L8
IPI00127866	Syt10	Mus muscu	synaptotagmin X
IPI00223738	OXSR1	Mus muscu	oxidative-stress responsive 1
IPI00314456	Klhdc8a	Mus muscu	kelch domain containing 8A
IPI00453913	PKHD1	Mus muscu	polycystic kidney and hepatic disease 1
IPI00131915	ubfd1	Mus muscu	ubiquitin family domain containing 1
IPI00123886	PRKDC	Mus muscu	protein kinase, DNA activated, catalytic polypeptide
IPI00129918	Smn1	Mus muscu	survival motor neuron 1
IPI00608064	FECH	Mus muscu	ferrochelatase
IPI00111827	snx6	Mus muscu	similar to sorting nexin 6; sorting nexin 6
IPI00123881	MCM6	Mus muscu	minichromosome maintenance deficient 6 (MIS5 homolog, S. pombe) (S. cerevisiae)
IPI00129911	NRP2	Mus muscu	neuropilin 2
IPI00314467	PSMB3	Mus muscu	proteasome (prosome, macropain) subunit, beta type 3
IPI00453924	RPL37	Mus muscu	ribosomal protein L37
IPI00346482	Cdh10	Mus muscu	cadherin 10
IPI00317340	LTF	Mus muscu	lactotransferrin
IPI00131909	pno1	Mus muscu	partner of NOB1 homolog (S. cerevisiae)
IPI00129908	CTNNAL1	Mus muscu	catenin (cadherin associated protein), alpha-like 1
IPI00129907	ACBD3	Mus muscu	acyl-Coenzyme A binding domain containing 3
IPI00123891	CSRP1	Mus muscu	cysteine and glycine-rich protein 1
IPI00110781	Ino80b	Mus muscu	INO80 complex subunit B
IPI00226249	ccdc104	Mus muscu	coiled-coil domain containing 104
IPI00223793	TRAF3IP3	Mus muscu	TRAF3 interacting protein 3
IPI00111831	Naca	Mus muscu	nascent polypeptide-associated complex alpha polypeptide
IPI00226289	OBFC1	Mus muscu	oligonucleotide/oligosaccharide-binding fold containing 1
IPI00108844	M6PR	Mus muscu	mannose-6-phosphate receptor, cation dependent
IPI00322509	MYRIP	Mus muscu	myosin VIIA and Rab interacting protein
IPI00108849	ST3GAL1	Mus muscu	ST3 beta-galactoside alpha-2,3-sialyltransferase 1
IPI00317356	PON1	Mus muscu	paraoxonase 1
IPI00648306	Col16a1	Mus muscu	collagen, type XVI, alpha 1
IPI00111807	F8	Mus muscu	coagulation factor VIII
IPI00222120	4930526D	Mus muscu	RIKEN cDNA 4930526D03 gene
IPI00123868	Phf2	Mus muscu	PHD finger protein 2
IPI00123867	LEMD3	Mus muscu	LEM domain containing 3
IPI00110753	Gm7172	Mus muscu	predicted gene 7172; similar to tubulin, alpha 1; tubulin, alpha 1A
IPI00222107	Frmd4a	Mus muscu	FERM domain containing 4A
IPI00265305	MCF2	Mus muscu	mcf.2 transforming sequence
IPI00453946	PNKD	Mus muscu	paroxysmal nonkinesiogenic dyskinesia
IPI00453949	4732471D1	Mus muscu	RIKEN cDNA 4732471D19 gene
IPI00265303	SAMD9L	Mus muscu	sterile alpha motif domain containing 9-like
IPI00123870	Smc1a	Mus muscu	structural maintenance of chromosomes 1A
IPI00281344	GXYLT1	Mus muscu	glycosyltransferase 8 domain containing 3
IPI00123871	ncor2	Mus muscu	nuclear receptor co-repressor 2
IPI00110762	PGC	Mus muscu	progastricsin (pepsinogen C)
IPI00110760	Dnajb4	Mus muscu	DnaJ (Hsp40) homolog, subfamily B, member 4
IPI00309309	Ell	Mus muscu	elongation factor RNA polymerase II
IPI00653912	Gm7092	Mus muscu	predicted gene 7092
IPI00653910	Cic	Mus muscu	capicua homolog (Drosophila)
IPI00466570	tmed10	Mus muscu	transmembrane emp24-like trafficking protein 10 (yeast); predicted gene 4024
IPI00108937	D16H22S6	Mus muscu	DNA segment, Chr 16, human D22S680E, expressed
IPI00553528	Gm5631	Mus muscu	predicted gene 5631
IPI00653927	TRUB1	Mus muscu	TruB pseudouridine (psi) synthase homolog 1 (E. coli)
IPI00132067	FBLN2	Mus muscu	fibulin 2
IPI00653921	rdx	Mus muscu	radixin
IPI00309322	Hmox2	Mus muscu	heme oxygenase (decycling) 2
IPI00131881	ADAM10	Mus muscu	a disintegrin and metallopeptidase domain 10
IPI00132076	COMT1	Mus muscu	catechol-O-methyltransferase 1
IPI00652969	ZFP91	Mus muscu	Zfp91-Cntf readthrough transcript; zinc finger protein 91; ciliary neurotrophic factor
IPI00139364	sfrs4	Mus muscu	splicing factor, arginine/serine-rich 4 (SRp75)
IPI00132080	pgls	Mus muscu	6-phosphogluconolactonase
IPI00132089	prep	Mus muscu	prolyl endopeptidase
IPI00131895	Gm7684	Mus muscu	predicted gene 7684; membrane-associated ring finger (C3HC4) 5
IPI00229425	CC2D2A	Mus muscu	coiled-coil and C2 domain containing 2A
IPI00131896	Gm3982	Mus muscu	brain protein 44; similar to brain protein 44; predicted gene 3982
IPI00125698	Lats2	Mus muscu	large tumor suppressor 2
IPI00318841	LOC10004	Mus muscu	predicted gene 4462; similar to eukaryotic translation elongation factor 1 gamma; predicted gene 9276; predicte
IPI00229432	BPTF	Mus muscu	bromodomain PHD finger transcription factor
IPI00263157	NOXO1	Mus muscu	NADPH oxidase organizer 1
IPI00229430	RPGRIP1L	Mus muscu	Rpgrip1-like
IPI00350458	UNC45B	Mus muscu	unc-45 homolog B (C. elegans)
IPI00223713	Hist1h1c	Mus muscu	histone cluster 1, H1c
IPI00469103	LOC63103	Mus muscu	similar to lysyl-tRNA synthetase; lysyl-tRNA synthetase
IPI00223714	Hist1h1e	Mus muscu	histone cluster 1, H1e
IPI00112963	Ctnna1	Mus muscu	catenin (cadherin associated protein), alpha 1
IPI00132011	4921530L2	Mus muscu	RIKEN cDNA 4921530L21 gene
IPI00314502	Tcfeb	Mus muscu	transcription factor EB
IPI00459725	idh3a	Mus muscu	isocitrate dehydrogenase 3 (NAD+) alpha
IPI00329839	DDX42	Mus muscu	DEAD (Asp-Glu-Ala-Asp) box polypeptide 42
IPI00469114	Hba-a1	Mus muscu	hemoglobin alpha, adult chain 2; hemoglobin alpha, adult chain 1
IPI00329837	TTC9C	Mus muscu	tetratricopeptide repeat domain 9C
IPI00469110	EML5	Mus muscu	echinoderm microtubule associated protein like 5
IPI00467793	4931406P1	Mus muscu	RIKEN cDNA 4931406P16 gene
IPI00131871	COPS4	Mus muscu	COP9 (constitutive photomorphogenic) homolog, subunit 4 (Arabidopsis thaliana)
IPI00453999	NCK1	Mus muscu	non-catalytic region of tyrosine kinase adaptor protein 1
IPI00474783	ACACA	Mus muscu	predicted gene 5182; acetyl-Coenzyme A carboxylase alpha
IPI00311920	LOC67721	Mus muscu	similar to U2AF homology motif (UHM) kinase 1; U2AF homology motif (UHM) kinase 1
IPI00265352	GPT2	Mus muscu	glutamic pyruvate transaminase (alanine aminotransferase) 2
IPI00453992	ATP6V1C2	Mus muscu	ATPase, H+ transporting, lysosomal V1 subunit C2
IPI00329840	RAD21	Mus muscu	RAD21 homolog (S. pombe)
IPI00379424	NEB	Mus muscu	nebulin
IPI00353203	tekt3	Mus muscu	tektin 3
IPI00467789	BRPF1	Mus muscu	bromodomain and PHD finger containing, 1
IPI00453996	MYH14	Mus muscu	myosin, heavy polypeptide 14
IPI00139378	UFM1	Mus muscu	ubiquitin-fold modifier 1
IPI00132039	Gm2199	Mus muscu	mitochondrial carrier homolog 2 (C. elegans); predicted gene, 100039384; predicted gene, 100039506
IPI00131845	Psma6	Mus muscu	proteasome (prosome, macropain) subunit, alpha type 6
IPI00112947	KRT19	Mus muscu	keratin 19
IPI00329848	abca5	Mus muscu	ATP-binding cassette, sub-family A (ABC1), member 5
IPI00653931	FAH	Mus muscu	fumarylacetoacetate hydrolase
IPI00311910	FBXO9	Mus muscu	f-box protein 9
IPI00314523	Bmp10	Mus muscu	bone morphogenetic protein 10
IPI00226311	TNRC6B	Mus muscu	trinucleotide repeat containing 6b
IPI00226310	COL6A6	Mus muscu	RIKEN cDNA E330026B02 gene
IPI00353237	TNS3	Mus muscu	tensin 3
IPI00265386	FAF2	Mus muscu	Fas associated factor family member 2
IPI00311914	ube4a	Mus muscu	ubiquitination factor E4A, UFD2 homolog (S. cerevisiae)
IPI00265380	MYH8	Mus muscu	myosin, heavy polypeptide 8, skeletal muscle, perinatal
IPI00132045	Trpc4	Mus muscu	transient receptor potential cation channel, subfamily C, member 4
IPI00226313	USP38	Mus muscu	ubiquitin specific peptidase 38
IPI00132042	Gm6123	Mus muscu	predicted gene 6123; pyruvate dehydrogenase (lipoamide) beta
IPI00314513	TMEM205	Mus muscu	transmembrane protein 205
IPI00132050	LOC67585	Mus muscu	NADH dehydrogenase (ubiquinone) 1, subcomplex unknown, 2; similar to NADH dehydrogenase (ubiquinone) 1,
IPI00468814	Erbb3	Mus muscu	v-erb-b2 erythroblastic leukemia viral oncogene homolog 3 (avian)
IPI00265379	TSC22D3	Mus muscu	TSC22 domain family, member 3
IPI00329876	gxylt2	Mus muscu	glycosyltransferase 8 domain containing 4
IPI00229485	tcerg1	Mus muscu	transcription elongation regulator 1 (CA150)
IPI00229483	SEC24C	Mus muscu	Sec24 related gene family, member C (S. cerevisiae)
IPI00329872	COL1A1	Mus muscu	collagen, type I, alpha 1
IPI00230277	MAPK3	Mus muscu	mitogen-activated protein kinase 3
IPI00229481	rgs12	Mus muscu	regulator of G-protein signaling 12
IPI00133103	CREG1	Mus muscu	cellular repressor of E1A-stimulated genes 1
IPI00222090	SH3PXD2B	Mus muscu	SH3 and PX domains 2B
IPI00112920	2700049A	Mus muscu	RIKEN cDNA 2700049A03 gene
IPI00222096	Dtx4	Mus muscu	deltex 4 homolog (Drosophila)
IPI00153875	RUFY2	Mus muscu	RUN and FYVE domain-containing 2
IPI00153874	Gtf2b	Mus muscu	general transcription factor IIB
IPI00320065	Cd1d1	Mus muscu	CD1d1 antigen; CD1d2 antigen
IPI00230263	Dgcr14	Mus muscu	DiGeorge syndrome critical region gene 14
IPI00604835	LOC10004	Mus muscu	predicted gene 2927; predicted gene 2849; predicted gene 2799; germ cell-less-like; predicted gene 2933; predic
IPI00230262	COL9A1	Mus muscu	collagen, type IX, alpha 1
IPI00651865	PHB2	Mus muscu	prohibitin 2
IPI00225201	iars	Mus muscu	isoleucine-tRNA synthetase
IPI00133110	TXNDC12	Mus muscu	thioredoxin domain containing 12 (endoplasmic reticulum)
IPI00752312	PRDM11	Mus muscu	PR domain containing 11
IPI00125630	gatA5	Mus muscu	GATA binding protein 5
IPI00225209	ILVBL	Mus muscu	ilvB (bacterial acetolactate synthase)-like
IPI00649807	psmd3	Mus muscu	proteasome (prosome, macropain) 26S subunit, non-ATPase, 3
IPI00759881	ACAD9	Mus muscu	acyl-Coenzyme A dehydrogenase family, member 9
IPI00225222	Nlrp4a	Mus muscu	NLR family, pyrin domain containing 4A
IPI00230296	LRRC41	Mus muscu	leucine rich repeat containing 41
IPI00130751	gck	Mus muscu	glucokinase
IPI00468850	Fahd1	Mus muscu	fumarylacetoacetate hydrolase domain containing 1
IPI00112904	Mmp2	Mus muscu	matrix metallopeptidase 2
IPI00130754	efnb1	Mus muscu	ephrin B1
IPI00283600	SLC25A23	Mus muscu	solute carrier family 25 (mitochondrial carrier; phosphate carrier), member 23
IPI00553590	Etl4	Mus muscu	enhancer trap locus 4
IPI00153893	Nags	Mus muscu	N-acetylglutamate synthase
IPI00225231	ank2	Mus muscu	ankyrin 2, brain
IPI00467729	Zfp462	Mus muscu	zinc finger protein 462
IPI00468859	Fads1	Mus muscu	fatty acid desaturase 1
IPI00230283	GFM1	Mus muscu	G elongation factor, mitochondrial 1
IPI00153894	SLC30A5	Mus muscu	solute carrier family 30 (zinc transporter), member 5
IPI00133132	PTK2B	Mus muscu	PTK2 protein tyrosine kinase 2 beta
IPI00757607	Zfp518	Mus muscu	zinc finger protein 518
IPI00662936	TMEM132	Mus muscu	transmembrane protein 132B
IPI00267661	BCL9	Mus muscu	B-cell CLL/lymphoma 9
IPI00267667	6330409N	Mus muscu	RIKEN cDNA 6330409N04 gene
IPI00320016	nonO	Mus muscu	non-POU-domain-containing, octamer binding protein; predicted gene 8806
IPI00125670	Med15	Mus muscu	mediator complex subunit 15
IPI00474711	PKN1	Mus muscu	protein kinase N1
IPI00125662	SMARCC1	Mus muscu	SWI/SNF related, matrix associated, actin dependent regulator of chromatin, subfamily c, member 1; predicted g
IPI00553576	abcd3	Mus muscu	ATP-binding cassette, sub-family D (ALD), member 3
IPI00469188	ADAMTS4	Mus muscu	a disintegrin-like and metallopeptidase (reprolysin type) with thrombospondin type 1 motif, 4
IPI00125667	TEP1	Mus muscu	telomerase associated protein 1
IPI00553577	2010111I0	Mus muscu	RIKEN cDNA 2010111I01 gene
IPI00345467	Gm382	Mus muscu	predicted gene 382
IPI00651893	AI747448	Mus muscu	expressed sequence AI747448
IPI00133163	Gm13453	Mus muscu	ATPase, H+ transporting, lysosomal V1 subunit G1; predicted gene 13453; predicted gene 12344
IPI00620900	ALK	Mus muscu	anaplastic lymphoma kinase
IPI00309361	RBP3	Mus muscu	retinol binding protein 3, interstitial
IPI00753494	WDR66	Mus muscu	WD repeat domain 66
IPI00125681	PIGS	Mus muscu	phosphatidylinositol glycan anchor biosynthesis, class S
IPI00469195	Echdc2	Mus muscu	enoyl Coenzyme A hydratase domain containing 2
IPI00270870	chd3	Mus muscu	chromodomain helicase DNA binding protein 3
IPI00133158	hipk1	Mus muscu	homeodomain interacting protein kinase 1; similar to protein kinase Myak-S
IPI00307837	Gm7161	Mus muscu	predicted gene 5869; predicted gene 7161; predicted gene 7105; predicted gene 5822; similar to eukaryotic tran
IPI00350425	CACHD1	Mus muscu	cache domain containing 1; similar to Cache domain containing 1
IPI00133172	Serpinb11	Mus muscu	serine (or cysteine) peptidase inhibitor, clade B (ovalbumin), member 11
IPI00320034	POLR2B	Mus muscu	polymerase (RNA) II (DNA directed) polypeptide B
IPI00229465	uaca	Mus muscu	uveal autoantigen with coiled-coil domains and ankyrin repeats
IPI00130794	TNXB	Mus muscu	tenascin XB
IPI00133167	Gm9803	Mus muscu	predicted gene 9803; mitochondria-associated protein involved in granulocyte-macrophage colony-stimulating f
IPI00261188	IFI35	Mus muscu	interferon-induced protein 35

r to ribosomal protein S28; predicted gene 10263; predicted gene 3511; ribosomal protein

glutamate oxaloacetate transaminase 1, solubl

; predicted gene 3200; predicted gene 12070; predicted gene 7286; predicted gene 6946; predicted gene 8825; predicted gene 9081; glyceraldehyde-3-phosphate dehydrogenase; p

LOC100044223; predicted gene 5506; predicted gene 5855; hypothetical protein LOC10004

); predicted gene 5562; glutathione S-transferase, mu

translocase 2 (Adenine nucleotide translocator 2) (ANT 2) (ADP,ATP carrier protein 2) (Solute carrier family 25 member 5); predicted gene 5529; predicted gene 8429; predicted gene

gene 13215; predicted gene 6111; predicted gene 7808; predicted gene 6014; predicted gene 8317; ubiquitin C; ubiquitin B; similar to fusion protein: ubiquitin (bases 43_513); ribosc

ruvate kina

450, family 2, subfamily c, polypeptide 69; cytochrome P450, family 2, subfamily c, polypeptide

G(i), alpha-2 subunit (Adenylate cyclase-inhibiting G alpha prot

r 2) (TRB2); taste receptor, type 2, member 10

ed gene 5525; eukaryotic translation elongation factor 1 gamma; similar to Elongation factor 1-gamma (EF-1-gamma) (eEF-1B gamma); predicted gene 43

subcomplex unknow

cted gene 2777; predicted gene 3706; predicted gene 14351; predicted gene 14367; predicted gene 2863; predicted gene 3701; predicted gene 14374; predicted gene 2784; predict

gene 700

slation elongation factor 1 alpha 1; predicted gene 6192; predicted gene 6392; predicted gene 6767; predicted gene 6170; predicted gene 6548; predicted gene 6789; eukaryotic tra

actor signal transducti

reduced gene 12319; predicted gene 12318; predicted gene 7784; predicted gene 12516; predicted gene 14148; predicted gene 13882; predicted gene 6217; predicted gene 7183; p

+1

eral proteins 127b (lower 217_152); similar to ubiquitin B; predicted gene 8609; ribosomal protein 127b; predicted gene 13317; predicted gene 13808; predicted gene 8430; RIKEN c

nd gene 2966; predicted gene 14166; predicted gene 14165; predicted gene 2829; predicted gene 14167; germ cell-less homolog 1 (Drosophila)-like; predicted gene 10921; predicte

eukaryotic elongation factor 1 alpha

predicted gene 10313; predicted gene 2467; predicted gene 5787; predicted gene 2193; predicted gene 13292; predicted gene, 380687; predicted gene 2076; predicted gene 3222;

:DNA 2810422J05 gene; similar to Ubc protein; predicted gene 13815; ubiquitin A-52 residue ribosomal protein fusion product 1; predicted gene 8797; predicted gene 1821; predicte

:d gene 3750; predicted gene 2913; hypothetical protein LOC100044046; predicted gen

predicted gene 7537, predicted gene 7293, predicted gene 11191, predicted gene_674224, predicted gene 12260, predicted gene 8200, similar to hCG1978856, predicted gene 2171

ed gene 11709, predicted gene 5239, predicted

6, similar to glyceraldehyde-3-phosphate dehydrogenase; predicted gene 7525, predicted gene 12233, predicted gene 3272, predicted gene 3310, predicted gene 2328, predicted gene 5839, predicted gene 9261, predicted gene

Term	Count	%	PValue	Genes	List Total	Pop Hits	Pop Total	Fold Enrichmer	Bonferroni	Benjamini	FDR	
GO:0005739~mitochondrion	24	30.3797468	0.004547	IPI00120719, IPI00132076, IPI00116748, IPI0011968	71	740	3842	1.75500571	0.490584335	0.106326838	5.28484634	No significantly enriched ter
GO:0044429~mitochondrial part	12	15.1898734	0.04161727	IPI00120719, IPI00116748, IPI00119685, IPI0012327	71	340	3842	1.909859155	0.998147455	0.269889753	39.7361633	No significantly enriched ter
GO:0005743~mitochondrial inner membrane	9	11.3924051	0.03811781	IPI00120719, IPI00119685, IPI00123276, IPI0031418	71	213	3842	2.286451101	0.996822843	0.287046669	37.0616456	No significantly enriched ter

ms
ms
ms

Term	Count	%	PValue	Genes	List Total	Pop Hits	Pop Total	Fold Enrich	Bonferroni	Benjamini	FDR	
GO:0005743~mitochondrial inner membrane	65	25	9.58E-31	IPI00133215, IPI0013	230	213	3842	5.097571	2.49E-28	2.49E-28	1.25E-27	significant enrichment
GO:0031966~mitochondrial membrane	68	26.15385	8.49E-29	IPI00133215, IPI0013	230	251	3842	4.525481	2.21E-26	7.36E-27	1.11E-25	significant enrichment
GO:0005740~mitochondrial envelope	69	26.53846	1.49E-28	IPI00133215, IPI0013	230	261	3842	4.416092	3.88E-26	9.70E-27	1.95E-25	significant enrichment
GO:0044429~mitochondrial part	74	28.46154	5.21E-25	IPI00133215, IPI0012	230	340	3842	3.635652	1.35E-22	2.26E-23	6.81E-22	significant enrichment
GO:0005739~mitochondrion	102	39.23077	3.77E-19	IPI00123276, IPI0011	230	740	3842	2.302491	9.80E-17	1.22E-17	4.92E-16	significant enrichment
GO:0070469~respiratory chain	24	9.230769	3.17E-16	IPI00133240, IPI0013	230	49	3842	8.181721	8.66E-14	9.66E-15	4.33E-13	significant enrichment
GO:0022900~electron transport chain	26	10	1.62E-14	IPI00133215, IPI0011	214	77	4147	6.543391	1.47E-11	4.90E-12	2.53E-11	significant enrichment
GO:0044455~mitochondrial membrane part	14	5.384615	6.77E-09	IPI00125460, IPI0012	230	31	3842	7.543899	1.76E-06	1.47E-07	8.85E-06	significant enrichment
GO:0006119~oxidative phosphorylation	10	3.846154	1.58E-05	IPI00230507, IPI0012	214	31	4147	6.251131	0.01417	0.00285	0.024572	significant enrichment

Term	Count	%	PValue	Genes	List Total	Pop Hits	Pop Total	Fold Enrichme	Bonferroni	Benjamini	FDR	
GO:0005743~mitochondrial inner membrane	71	40.3409091	4.65E-49	IPI00120719,	161	213	3842	7.95445135	9.62E-47	9.62E-47	5.86E-46	significant enrichment
GO:0031966~mitochondrial membrane	74	42.0454545	3.89E-47	IPI00120719,	161	251	3842	7.03541115	8.06E-45	2.69E-45	4.91E-44	significant enrichment
GO:0005740~mitochondrial envelope	74	42.0454545	8.68E-46	IPI00120719,	161	261	3842	6.76585517	1.80E-43	4.49E-44	1.09E-42	significant enrichment
GO:0044429~mitochondrial part	76	43.1818182	4.01E-39	IPI00120719,	161	340	3842	5.33416149	8.30E-37	1.38E-37	5.06E-36	significant enrichment
GO:0005739~mitochondrion	91	51.7045455	1.61E-26	IPI00120719,	161	740	3842	2.93454759	3.32E-24	4.16E-25	2.02E-23	significant enrichment
GO:0022900~electron transport chain	24	13.6363636	2.18E-16	IPI00133240,	145	77	4147	8.91428571	1.36E-13	4.54E-14	3.33E-13	significant enrichment
GO:0070469~respiratory chain	20	11.3636364	1.31E-14	IPI00133240,	161	49	3842	9.74014451	2.71E-12	3.01E-13	1.65E-11	significant enrichment
GO:0045333~cellular respiration	15	8.52272727	2.52E-10	IPI00331332,	145	47	4147	9.12765957	1.55E-07	3.86E-08	3.73E-07	significant enrichment
GO:0055085~transmembrane transport	26	14.7727273	3.14E-10	IPI00125460,	145	169	4147	4.4	1.93E-07	3.86E-08	4.65E-07	significant enrichment
GO:0044455~mitochondrial membrane part	12	6.81818182	1.91E-08	IPI00125460,	161	31	3842	9.23742737	3.96E-06	3.04E-07	2.41E-05	significant enrichment
GO:0006119~oxidative phosphorylation	11	6.25	4.43E-08	IPI00125460,	145	31	4147	10.1483871	2.72E-05	3.89E-06	6.57E-05	significant enrichment
GO:0022904~respiratory electron transport chain	9	5.11363636	3.69E-07	IPI00331332,	145	22	4147	11.7	2.26E-04	2.83E-05	5.46E-04	significant enrichment
GO:0003954~NADH dehydrogenase activity	8	4.54545455	3.13E-06	IPI00308882,	147	20	4133	11.2462585	8.90E-04	1.27E-04	0.00415362	significant enrichment
GO:0050136~NADH dehydrogenase (quinone) activity	8	4.54545455	3.13E-06	IPI00308882,	147	20	4133	11.2462585	8.90E-04	1.27E-04	0.00415362	significant enrichment
GO:0008137~NADH dehydrogenase (ubiquinone) activ	8	4.54545455	3.13E-06	IPI00308882,	147	20	4133	11.2462585	8.90E-04	1.27E-04	0.00415362	significant enrichment
GO:0005741~mitochondrial outer membrane	11	6.25	3.46E-05	IPI00122549,	161	51	3842	5.14699793	0.00712889	3.97E-04	0.04355489	significant enrichment

Upregulated mitochondria-associated proteins (vs. LF)

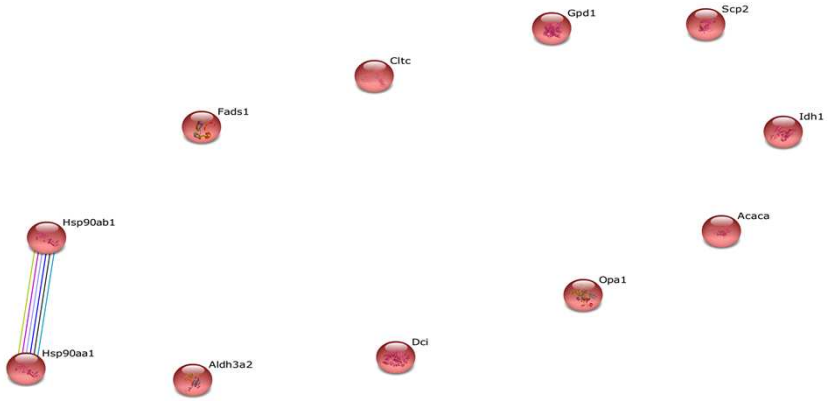

Downregulated mitochondria-associated proteins (vs. LF)

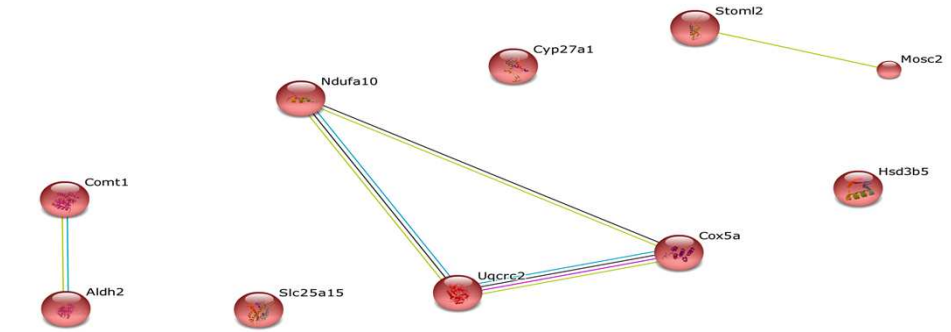

Upregulated mitochondria-associated proteins (vs. LF)

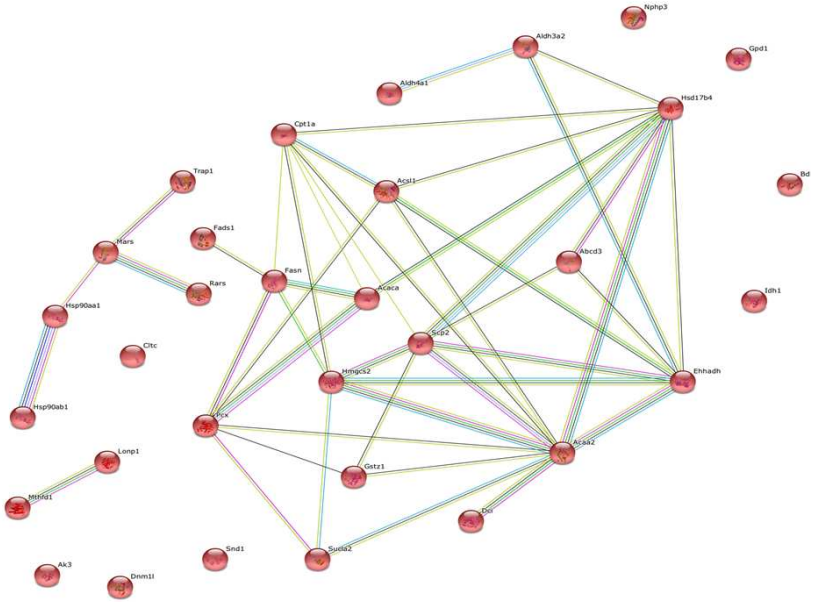

Downregulated mitochondria-associated proteins (vs. LF)

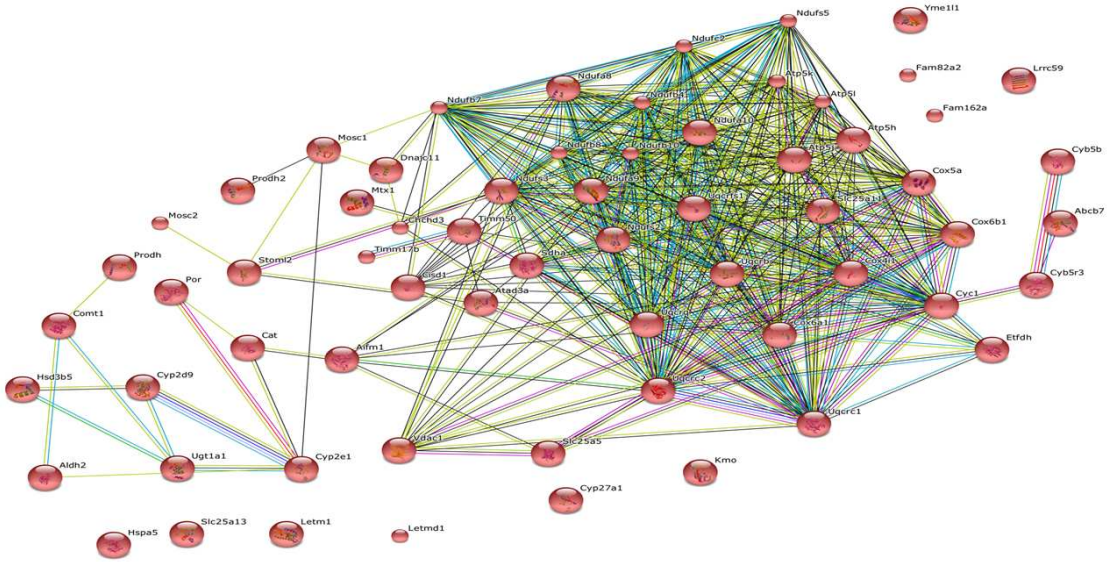

Upregulated mitochondria-associated proteins (vs. LF)

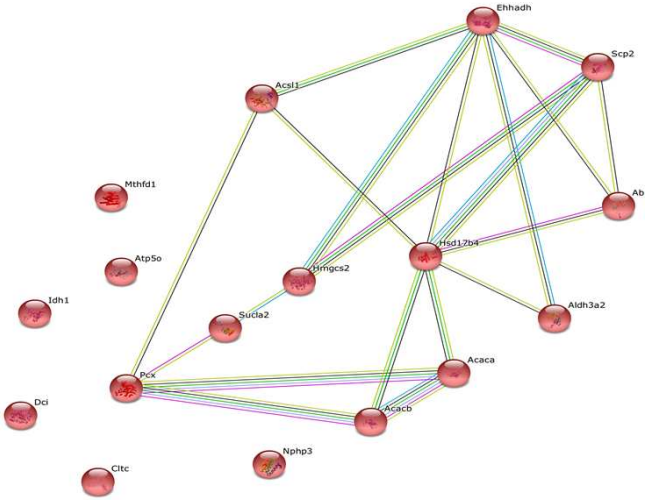

Downregulated mitochondria-associated proteins (vs. LF)